Atomic Layer Deposition of Inorganic–Organic Hybrid Material Thin Films

Leo D. Salmi

Department of Chemistry
Faculty of Science
University of Helsinki
Finland

DOCTORAL DISSERTATION

To be presented for public discussion with the permission of the Faculty of Science of the University of Helsinki, in Auditorium D101 of the Department of Physics, Gustaf Hällströmin katu 2, on the 4th of September, 2020 at 12 o'clock.

HELSINKI 2020

Supervisor

Professor Mikko Ritala
Department of Chemistry
University of Helsinki
Finland

Reviewers

Professor Alan W. Weimer
Department of Chemical and Biological Engineering
University of Colorado Boulder
USA

Assistant Professor Antti Karttunen
Department of Chemistry and Materials Science
Aalto University
Finland

Opponent

Professor Maarit Karppinen
Department of Chemistry and Materials Science
Aalto University
Finland

ISBN 978-951-51-6438-4 (paperback)
ISBN 978-951-51-6439-1 (PDF)
http://ethesis.helsinki.fi
Unigrafia
Helsinki 2020

"I'm just a simple man trying to make my way in the universe."
Jango Fett

Abstract

Inorganic–organic hybrids represent a class of materials consisting of inorganic and organic components mixed at the molecular level. This offers not only the possibility to combine material properties of the constituents, but also to discover completely new characteristics. Because of this, hybrid materials have become an important part of materials research.

Atomic layer deposition (ALD) is a gas phase thin film deposition method with the ability to deposit conformal films with good control over film thickness and composition. Furthermore, ALD offers large-area uniformity and perfect step-coverage. Molecular layer deposition (MLD), used for depositing organic polymers, is a method derived directly from ALD. The combination of ALD and MLD offers a convenient way of depositing inorganic–organic hybrid material thin films for applications, such as electronics and optics, where ultimate precision is needed. In this thesis, ALD/MLD was used to deposit hybrid nanolaminates, metal–organic frameworks, and zinc glutarate.

Nanolaminates of Ta_2O_5 and polyimide were deposited using tantalum ethoxide, water, pyromellitic dianhydride, and diaminohexane as the precursors. The leakage currents could be greatly reduced compared to the bare Ta_2O_5 and polyimide by layering of the materials. It was also shown that the mechanical properties could be improved by introduction of the organic layers.

MOF-5 and IRMOF-8 thin films were deposited using zinc acetate, 1,4-benzenedicarboxylic acid, and 2,6-naphthalenedicarboxylic acid as the precursors. The deposition process included ALD/MLD combined with a two-step post-deposition crystallization in moist air and in an autoclave with dimethylformamide. Despite the need for a liquid-phase crystallization, the conformality and continuity of the films could be preserved.

ALD/MLD of zinc glutarate thin films was shown for the first time ever using zinc acetate and glutaric acid as the precursors. The films were crystalline as-deposited

with a structure matching to zinc glutarate. Catalytic activity of the films was demonstrated by polymerizing propylene oxide and CO_2 in the presence of zinc glutarate coated glass wool and steel mesh.

Preface

The experimental work for this thesis was carried out in the Laboratory of Inorganic Chemistry at the University of Helsinki during years 2008–2017. The work was financially supported by the Academy of Finland (project 121325). ASM Microchemistry Ltd. is also acknowledged for funding my doctoral studies.

I am deeply grateful to Professors Mikko Ritala and Markku Leskelä for giving me the opportunity to work in one the leading ALD research groups. All these years with the best ALD experts made it possible to be where I am today. Special thanks go to Professor Mikko Ritala for his ultimate patience.

I would like to thank the reviewers Professor Alan W. Weimer and Assistant Professor Antti Karttunen for their useful comments. They helped me improving this thesis in a great many ways.

Thank you to my co-author and university roommate Mr. Mikko J. Heikkilä. You did amazing job with all the X-ray related characterization. You always have time for others on your to-do list. Thanks for not kicking me out the office after leaving the University.

I am very thankful for all the other people who contributed to the publications of this thesis. Thank you Dr. Esa Puukilainen and Mr. Miika Mattinen for your expertise in AFM. Dr. Marko Vehkamäki is thanked for introducing me the secrets of electrical characterization and FIB-SEM imaging. Prof. Timo Sajavaara, Dr. Kenichiro Mizohata, and Prof. Jyrki Räisänen are acknowledged for all the TOF-ERDA measurements and related analysis. Dr. David Grosso is thanked for the porosity measurements. I owe a big thanks to Dr. Teemu Niemi, Dr. Sami-Pekka Hirvonen, and Ms. Sanna Korhonen for their help with the polymerization experiments and polymer characterization under a very tight schedule. Finally, I would like to thank Dr. Marianna Kemell for her invaluable help with the FESEM and EDS.

My heartfelt thanks go to all the people who have been part of the Laboratory of Inorganic Chemistry at the University of Helsinki during all these years. Thank you Dr. Timo Hatanpää, Dr. Jaakko Niinistö, and Dr. Antti Niskanen for helping me with the first steps in the world of ALD. The quartermaster Dr. Jani Hämäläinen was always ready to help with reactor related questions and kept the spares inventory full. I want to thank all the colleagues from the lab for creating such a nice work environment. Finally, thank you Dr. Miia Mäntymäki for being a good friend to me and my family on and off work.

Thanks to all the people who have made the Friday floorball (or maybe "sähly" is a more describing word) matches so much fun. The honorable mention goes to the Kumpula Private Badminton Club. Thanks Marko, Jaakko, and Hannu.

I would like to thank my parents Helena and Markku for their love and support in life. You have always gently kicked me in the right direction whenever needed. Thank you also Aimo, Pirkko, Hanna, Iida, and Eeva for making me feel like part of the family from the beginning.

The warmest appreciation and love goes to my family; my daughter Ella and especially my wife Emma. You have been there for the best and the worst with never ending love and understanding. Also, thank you Tera for being a stereotypical Chihuahua and never wanting to go on a 10 km walk 5 o'clock in the morning through wind and rain.

Espoo, January 2020

Leo D. Salmi

List of Original Publications

I L. D. Salmi, E. Puukilainen, M. Vehkamäki, M. Heikkilä, and M. Ritala: Atomic Layer Deposition of Ta_2O_5/Polyimide Nanolaminates, Chemical Vapor Deposition 2009, 15, 221–226.

II L. D. Salmi, M. J. Heikkilä, E. Puukilainen, T. Sajavaara, D. Grosso, and M. Ritala: Studies on Atomic Layer Deposition of MOF-5 Thin Films, Microporous and Mesoporous Materials, 2013, 182, 147–154.

III L. D. Salmi, M. J. Heikkilä, M. Vehkamäki, E. Puukilainen, M. Ritala, and T. Sajavaara: Studies on Atomic Layer Deposition of IRMOF-8 Thin Films, Journal of Vacuum Science & Technology A, 2015, 33, 01A121-1–01A121-8.

IV L. D. Salmi, M. Mattinen, T. Niemi, Mikko J. Heikkilä, K. Mizohata, S. Korhonen, S.-P. Hirvonen, J. Räisänen, and M. Ritala: Atomic Layer Deposition of Zinc Glutarate Thin Films, Advanced Materials Interfaces, 2017, 4, 22, 1700512-1–1700512-6.

The author has done all the thin film depositions, growth characterization, and crystallization experiments in publications I–IV. Most of the FESEM imaging and EDS, GIXRD, and electrical measurements were also carried out by the author who also analyzed the results with the help of the co-authors. The author has written all the manuscripts and finalized them with the co-authors.

Other publications by the author:

1. J. Holopainen, M. J. Heikkilä, L. D. Salmi, K. Ainassaari, and M. Ritala: Zeolitic imidazole Framework-8 (ZIF-8) Fibers by Gas-Phase Conversion of Electroblown Zinc Oxide and Aluminum Doped Zinc Oxide Fibers, Microporous and Mesoporous Materials, 2018, 267, 212–220.

2. H. Lan, L. D. Salmi, T. Rönkkö, J. Parshintsev, M. Jussila, K. Hartonen, M. Kemell, and M-L. Riekkola: Integrated Atomic Layer Deposition and Chemical Vapor Reaction for the Preparation of Metal Organic Framework Coatings for Solid-Phase Microextraction Arrow, Analytica Chimica Acta, 2018, 1024, 93–100.

Contents

Abbreviations

3D	three-dimensional
Ac	acetate
a.u.	arbitrary unit
AFM	atomic force microscopy
APCVD	atmospheric pressure chemical vapor deposition
ALD	atomic layer deposition
BDC	benzenedicarboxylic acid
CMOS	complementary metal oxide semiconductor
CVD	chemical vapor deposition
DAH	diaminohexane
DEZ	diethyl zinc
DMF	dimethylformamide
EDS	energy-dispersive X-ray spectroscopy
EG	ethylene glycol
FESEM	field emission scanning electron microscopy
FTIR	fourier-transform infrared spectroscopy
GA	glutaric acid
GIXRD	grazing incidence X-ray diffraction
HTXRD	high-temperature X-ray diffraction
IRMOF	isoreticular metal–organic framework
ITO	indium tin oxide
L-B	Langmuir-Blodgett
LPCVD	low pressure chemical vapor deposition
MLD	molecular layer deposition
MOF	metal–organic framework
MOEP	metal octaethylporphyrin
NDC	naphthalenedicarboxylic acid
NMR	nuclear magnetic resonance
OEt	ethoxide
OPr	isopropoxide
Pc	tetra-t-butyl-Zn-phthalocyanine

PECVD	plasma enhanced chemical vapor deposition
PMDA	pyromellitic dianhydride
PVD	physical vapor deposition
q	8-hydroxyquinoline
RF	radio frequency
RH	relative humidity
SAM	self-assembled monolayer
SEC	size-exclusion chromatography
thd	2,2,6,6-tetramethyl-3,5-heptanedionate
TAS	dicitratodiperoxotitanate complex ammonium salt
TMA	trimethylaluminum
TOF-ERDA	time-of-flight elastic recoil detection analysis
UHCVD	ultrahigh vacuum chemical vapor deposition
UV	ultraviolet
Vis	visible
XRD	X-ray diffraction
XRR	X-ray reflection
ZIF	zeolitic imidazolate framework

1. Introduction

During the last three decades nanoscience has produced hundreds of new advanced functional materials to be used for example in electronics, optics, catalysis, protective coatings, and sensors. As the development of conventional inorganic and organic materials has become increasingly challenging due to limited options, inorganic–organic hybrid materials have gained considerable attention in the recent years. Mixing of inorganic and organic building blocks offers a nearly unlimited reservoir of new materials combining the properties of the constituents and even exhibiting completely new characteristics. Thus, hybrid materials will probably play an important role in overcoming the current limitations of the state-of-the-art technology such as size, environmental hazards, energy efficiency, reliability, and costs. Tailoring of hybrid materials often results in unpredictable and currently incomprehensible outcome of material properties opening up a vast field for basic research.

As new materials are being studied, the development of suitable synthesis methods is also of utmost importance. Properties of inorganic–organic hybrid materials are usually determined by proportions of the inorganic and organic constituents, thus requiring a precise control over material composition from the synthesis method. In some applications like electronics, optics, and magnetics, coating of complicated 3D structures with thin films ranging from a few to hundreds of nanometers is often needed. This requires good uniformity and step coverage, and the ability to control film thickness at nanometer level. The traditional liquid phase synthesis methods of hybrid materials, such as the sol–gel technique, leave a lot to be desired in this sense.

Atomic layer deposition (ALD) is an advanced thin film deposition technique related to chemical vapor deposition (CVD). It is based on saturative surface reactions during alternating pulses of gaseous precursors separated by inert gas purging. Each reaction step is saturative. This self-limiting growth mode results in good control over film thickness, large area uniformity, and perfect step-coverage. ALD technology was invented in 1974 by Suntola and co-workers for the manufacturing of electroluminescent flat panel displays and is nowadays used for example by Intel Corp.

in their integrated circuit manufacturing process. ALD of organic polymers is similar to conventional inorganic ALD. This method is also known as molecular layer deposition (MLD) as a layer of molecules instead of atoms is deposited during one reaction step. The combination of ALD and MLD is potentially a convenient method for deposition of various inorganic–organic hybrid materials as it can fulfill all the above-mentioned desired properties for hybrid thin film synthesis.

The goal of this work was to study the possibility of depositing different inorganic–organic hybrid materials by ALD/MLD and carry out basic characterization of electric, structural, compositional, and mechanical properties of the resulting films. Synthesis of metal–organic framework (MOF) thin films utilizing ALD was also shown for the first time. This thesis presents a literature review of common hybrid material thin film deposition methods. The basics of ALD and MLD are also introduced briefly. The experimental part describes the ALD/MLD processes used for the film deposition and the characterization methods applied. The results on deposition and characterization of Ta_2O_5/polyimide nanolaminates, MOF-5 and IRMOF-8 thin films, and zinc glutarate thin films are finally presented and discussed.[I–IV]

2. Background

2.1 Atomic Layer Deposition

Atomic layer deposition is a gas phase thin film deposition method related to chemical vapor deposition.[1] Whereas in traditional CVD the precursors are supplied simultaneously and react in the gas phase and on the substrate, ALD relies on saturative surface reactions during separate precursor pulses. The main idea of ALD is presented in Figure 1 with the $HfCl_4/H_2O$ process for HfO_2. The precursor vapors are led to the substrate one by one where they react with the surface. Once all the surface groups have reacted with the precursor, the substrate chamber is evacuated or purged with an inert gas to remove the released by-products and the excess precursor. Only thereafter the second precursor is delivered onto the substrate. Due to this kind of self-limiting growth mode the same amount of material is deposited during each ALD cycle independent of the precursor exposure time (Figure 2) and film thickness can be easily controlled by the number of cycles. The self-limiting growth also ensures large area uniformity, conformality, and good control over film composition.[2]

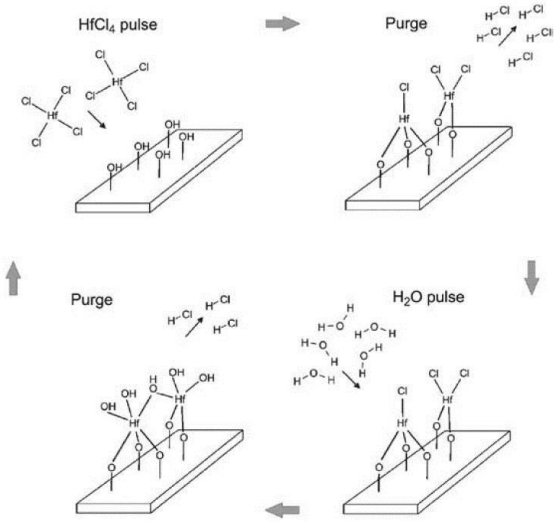

Figure 1. A schematic representation of one ALD cycle. In the example $HfCl_4$ and H_2O are used to deposit HfO_2. Reprinted from Ref. 2, with permission from The Royal Society of Chemistry.

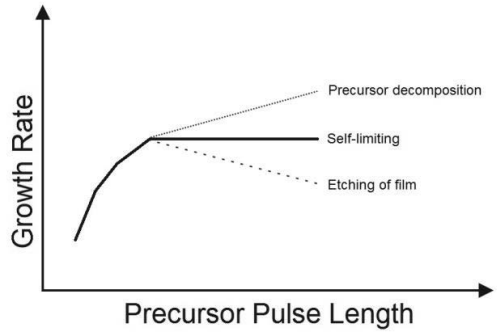

Figure 2. In the self-limiting ALD growth the increase in film thickness during one ALD cycle becomes independent of the precursor pulse length once the minimum value needed for saturation is exceeded. For example precursor decomposition or etching of the film can increase or decrease the growth rate.

Choosing the right precursors plays a crucial role in ALD. The precursors should be thermally stable to prevent CVD like growth but still as reactive as possible on the surface. If these requirements are not met, the self-limiting behavior is lost and the films can contain increased amounts of impurities. Volatility is also of utmost importance as the precursor source temperature should be well below the deposition temperature to prevent condensation. Other must have precursor requirements include no etching of or dissolution into the film or substrate and sufficient purity.[2]

In the ideal ALD one monolayer is deposited during each cycle. However, this is usually not the case as the growth is affected by steric hindrance of the precursor molecules, number of reaction sites on the surface, and unideal nucleation. In typical ALD processes the growth rates are usually below 2 Å/cycle. The deposition temperature region where the reactions are saturative and thus self-limiting is called "the ALD window" (Figure 3).[2] In the ALD window growth rate may or may not be temperature independent as surface coverages of the precursors are often dictated by the temperature. The characteristic linear dependency of film thickness on the number of cycles applied can also be absent for very thin films because of nucleation problems or accelerated growth in the beginning of the deposition on certain substrates. Once a continuous film is formed, the increase of thickness per cycle starts to follow the linear pattern.

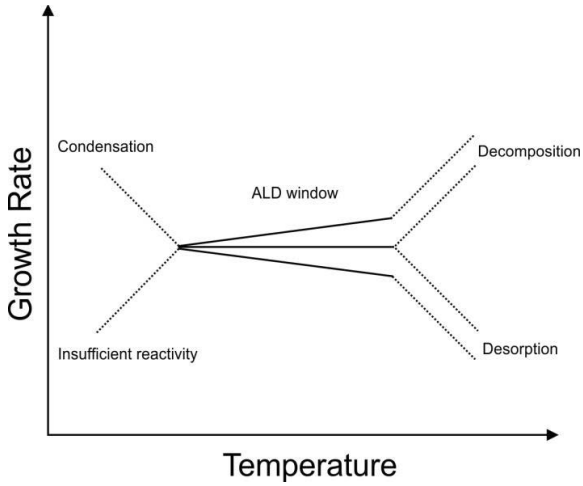

Figure 3. Typical temperature dependency of growth rate for an ideal ALD process.

The most common approaches to ALD have been binary processes of oxides, nitrides, and sulphides such as Al_2O_3, TiO_2, HfO_2, TaN, TiN, and ZnS.[3] However, several multicomponent materials have also been deposited including $BaTiO_3$,[4] $SrTiO_3$,[5] and $LaAlO_3$,[6] as well as laminates combining two materials in a composite structure.[7] The major drawback of ALD is the slow growth rate caused by the layer-by-layer nature of the method. This has limited the commercial use mostly to applications where ultimate precision and very thin films are needed. However, the first commercial application of ALD thin films was the use of ZnS and Al_2O_3 in electroluminescent displays patented in 1977.[8] In these devices the ALD made films have thicknesses from 200 nm to over a micrometer. Later the major driver for the industrialization of ALD has been the semiconductor industry. The search for replacement of SiO_2 as the transistor gate oxide culminated in 2007 when Intel adopted ALD as the manufacturing method for the high-k gate dielectric in their 45 nm CMOS devices.[9] As the industry is driven by downscaling of the device features, ALD has become increasingly important in realizing these goals. Some other industrial applications for ALD are protective, optic and biocompatible coatings, solar panels, and magnetic recording heads.[2]

2.2 Molecular Layer Deposition

Molecular layer deposition is a gas-phase thin film deposition method developed directly from ALD. In MLD layers of molecules instead of atoms are deposited in a layer-by-layer manner (Figure 4).[10] Because the building blocks are molecules, the growth rates are usually much higher than in traditional ALD processes. The different nature of organic precursors as well as the deposited polymer materials affect also other growth characteristics. For example the temperature dependency is usually much larger for the MLD processes, and the window for the constant growth rate is often very narrow or completely absent. This is often caused by desorption of the precursor molecules that are weakly bonded or not fully reacted on the surface. Also, many MLD made materials have intrinsic porosity, which can easily cause trapping of the precursor molecules inside the film especially at low temperatures leading to a CVD type of growth.[11]

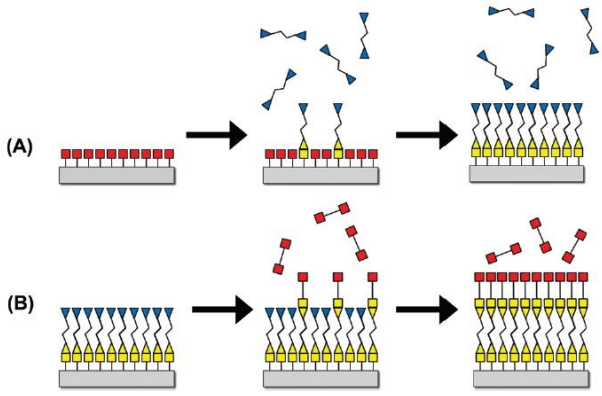

Figure 4. Schematic illustration of an MLD cycle. Reprinted from Ref. 10, with permission from ACS Publications.

Like in ALD, careful selection of precursors is very important in MLD. The large size of many organic molecules brings additional challenges to finding suitable precursors. Low vapor pressure is often the limiting factor, and decomposition of the precursor occurs before evaporation.[11] Another problem is that many polymeriza-

tion reactions are slow in the gas-phase and on the surface, whereas perfect MLD type of growth requires fast and complete reactions. This can lead into the above-mentioned desorption of the weakly bonded precursor molecules from the surface resulting in a low growth rate or no growth at all. Slow formation of covalent bonds on the surface can also affect the final material properties compared to bulk polymers. Third possible problem with organic precursors is double reaction during the precursor pulse.[11] This means that a non-rigid linear molecule reacts with the surface from its both ends. The result is a decreased growth rate or complete inhibition of the growth. To overcome this problem one may choose precursor molecules with different terminating groups or even modify the surface species *in situ* for example by ring opening reactions.

One of the first MLD processes was reported already in 1991 by Yoshimura et al.[12] Pyromellitic dianhydride was used with 2,4-diaminonitrobenzene or 4,4'-diaminodiphenyl ether to deposit polyamide films. Since then, several other organic polymers have been deposited utilizing MLD including polyimides[13], polyurea[14], polythiourea[15], and polyimines[16]. In the last few years, many MLD studies have concentrated on inorganic-organic hybrid materials. In the deposition of hybrid materials the conventional inorganic ALD and organic MLD are combined. This will be further discussed in Chapter *2.3.2.3*.

2.3 Inorganic–organic Hybrid Thin Films

The industrial era of inorganic–organic materials started already in the mid-20th century. Applications were found in places like paint, glass and metal industry. At the same time, the scientific community also started to show interest in inorganic–organic compounds leading to such innovations as silicones and organically templated zeolites.[17] However, it wasn't until the early 1980's before the sol–gel method started gaining more attention[18,19] and gave an easy pathway to synthesizing inorganic–organic hybrid thin films. Since then, several liquid- and gas-phase methods have emerged for the deposition of a vast variety of hybrid materials in the form

of thin films expanding their potential applications. The most common methods for hybrid thin film deposition will be discussed in more detail in Chapters 2.3.1 and 2.3.2.

2.3.1 Liquid-Phase Deposition

Liquid-phase synthesis is one of the simplest and cheapest ways of making thin films. No expensive high vacuum or precursor delivery systems are needed. The precursors are incorporated into the liquid phase and the substrate is contacted with the liquid. In some cases the precursor solution can be spread onto the substrate via spinning or spraying. Usually some kind of post-treatment, such as heating, is needed to further improve properties of the film. In the following chapters some of the most common liquid-phase methods for depositing inorganic–organic hybrid thin films are discussed.

2.3.1.1 Sol–Gel

Sol–gel technique offers mild processing conditions suitable for organic precursors and film materials. Therefore it is one of the most studied and used techniques for synthesizing inorganic–organic hybrid materials.[20] Due to the possibility of spin- or dip-coating the precursor sol onto a substrate, it is also one the first methods used for preparing inorganic–organic thin films. Most of the sol–gel deposited hybrid thin film materials are ormosils, i.e. organically modified silicas, but for example zirconium[21,22] and titanium[23–25] containing films have been commonly reported. Potential applications range from electronic devices[26] and optical materials[27,28] to protective coatings[29].

Basic steps of the sol–gel method are illustrated in Figure 5.[30] The process is based on making a sol by mixing colloidal particles in a solvent or hydrolyzing alkoxides in water. The organic part can be added into the sol as a separate dopant or it can be bonded to the precursor molecule (e.g. organically modified alkoxides). This makes

sol–gel a convenient method for depositing hybrid thin films with easy control on constituents of the material. The transformation of a sol into a gel occurs through hydrolysis and condensation reactions. The formed gel needs an aging period, during which the particles form a network and solvent is removed from the material. The final steps are removal of the remaining solvent by heat and densification of the films at higher temperatures.

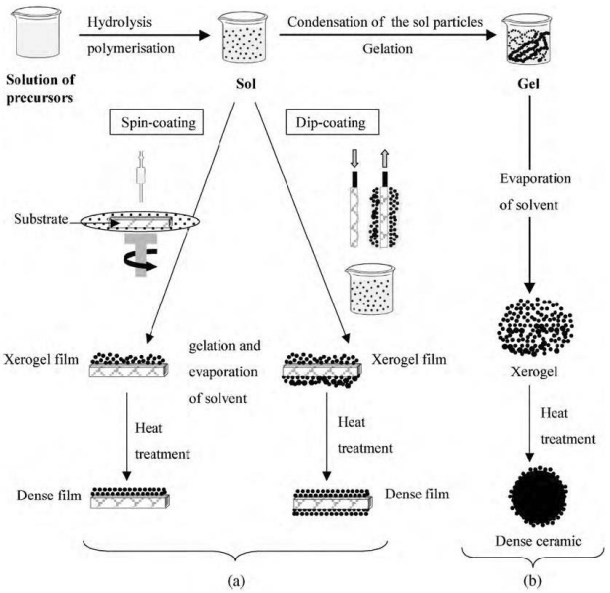

Figure 5. Basic steps of making thin films (a) or powders (b) by the sol–gel method. Reprinted from Ref. 30 with permission from Elsevier B.V.

The advantage of the sol–gel technique is that it is relatively cheap and simple. Even though the processes need heat, the thermal budget is usually low compared to other methods. Also, when making hybrid thin films the temperature is kept much lower compared to ceramic films. Sol–gel offers also the possibility to coat very large areas without complicated machinery e.g. vacuum equipment. The biggest problems with the sol–gel deposited thin films are usually related to cracking during the final heat treatment, which can be detrimental in protective coatings and optics.[31] However, it has been shown that this can be avoided if the film thickness is kept below the so-called critical thickness.[32]

2.3.1.2 Solvothermal Method

Solvothermal deposition of thin films relies on reactions of dissolved precursors on a substrate under moderate to high pressure and heat. While it is a simple method for making thin films, the energy budget can be very high, and the deposition time ranges from days to weeks. To overcome these weaknesses several strategies, including microwaves[33] and ultrasonification[34], have been implemented to assist the growth. Surface of the substrate also plays a crucial role as it needs to promote crystallization and anchor the film to the substrate. Thus, a pretreatment of the substrate is often needed. This is usually done by a deposition of a seed crystal layer or self-assembled monolayer (SAM).[35] As the film growth proceeds via a formation of separate crystallites, another issue with the solvothermal deposition has been poor continuity of the films. This is eminently true for very thin layers.

Despite its weaknesses, solvothermal synthesis has played an important role especially in depositing thin films of metal–organic frameworks (MOF), which is a group of highly porous and crystalline hybrid materials consisting of inorganic moieties connected with rigid organic linker molecules.[36–38] A good example is the isoreticular series of MOFs built from Zn_4O clusters connected by different carboxylates.[38,39] Some of these are depicted in Figure 6. Most of the studies on solvothermal growth of MOF films have concentrated on MOF-5,[33,40–43] but also reports on other MOFs, such as ZIF-8,[44,45] HKUST-1,[46] and CAU-1,[47] exist.

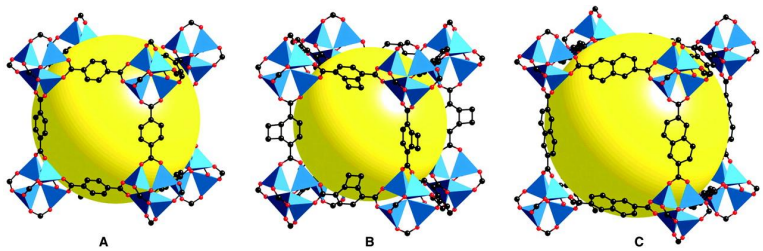

Figure 6. Schematic illustrations of A) MOF-5, B) IRMOF-6, and C) IRMOF-8. Yellow spheres represent the large pore size. Reprinted from Ref. 39, with permission from AAAS.

2.3.1.3 Langmuir-Blodgett Method

The Langmuir-Blodgett (L-B) method is based on a material transfer from a liquid-gas interface onto a solid substrate.[48] The substrate is immersed into the liquid vertically, and one or more monolayers are deposited onto the substrate (Figure 7).[49] This cycle can be repeated to achieve the desired film thickness. This offers a simple and cost effective way of making highly organized thin films with tunable composition.

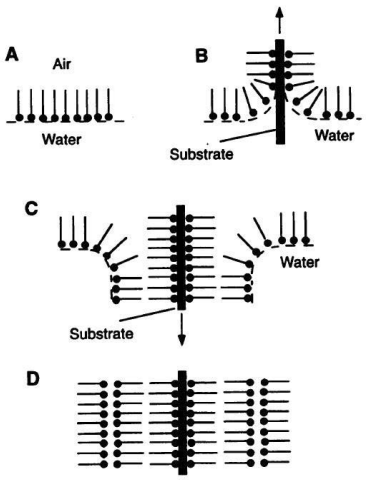

Figure 7. Schematic illustration of a conventional L-B film deposition process. The solution containing an amphiphilic molecule is spread on the liquid-gas interphase (A) and the substrate is then passed through the layer (B) and repeated to acquire the desired film thickness (C and D). Reprinted from Ref. 49, with permission from AAAS.

The molecules used in the L-B method are usually long hydrocarbon chains with hydrophilic and lipophilic ends, known as amphiphiles. This is also the weakness of the method as it narrows down the selection of materials. However, it has been shown that also some non-amphiphilic molecules can be used in the L-B method if they are mixed with fatty acids.[50] The acid works as a support for the molecule and enables the formation of an organized layer on the liquid-gas interphase. Other downsides of the L-B method are poor thermal and mechanical stability of the films and inhomogeneity on larger substrates.[51]

Despite the limited number of suitable molecules, the L-B method has been used to deposit several inorganic–organic hybrid materials. For example polyoxometalate containing hybrid amphiphiles have been reported by many groups as suitable molecules for the deposition of hybrid thin films.[52–55] Bhullar *et al.* prepared polyaniline-TiO_2 nanocomposites and used the L-B method to deposit polyaniline-TiO_2 hybrid thin films.[56] Another approach to making hybrid L-B films was presented by Usami *et al.* who used solutions of dicitratodiperoxotitanate complex ammonium salt (TAS) and tetra-*t*-butyl-Zn-phthalocyanine (Pc) to deposit Zn and Ti containing hybrids.[57] The Pc solution was first spread on the solution of TAS in a L-B trough. The hybrid film was then compressed and transferred onto the substrate.

2.3.2 Vapor Phase Deposition

Vapor phase deposition techniques rely on transfer of the thin film forming materials onto the substrate through a gas phase. The deposition process can be physical, where material condenses onto the substrate, or chemical reactions may take place to form the desired material. As a vacuum or low pressure environment is usually needed for vapor phase deposition, the equipment is often more complex and expensive than in the liquid-phase deposition. Especially the more advanced variations, such as ALD, need state of the art vacuum reactors, and are thus used only in applications where ultimate precision is needed. ALD and MLD were used to deposit all the materials in this thesis and will be further discussed in Chapter *2.3.2.3*. Generally the main challenge in depositing inorganic–organic hybrid materials by vapor phase techniques has been evaporating the organic part. Especially larger organic molecules tend to decompose before vaporization.

2.3.2.1 Physical Vapor Deposition

Physical vapor deposition (PVD) includes several thin film deposition techniques in which material is transferred from a condensed source or target to a gas phase, transported to the substrate under vacuum, and condensed into a film. The source

material can be solid or liquid and the transfer can be achieved by several ways.[58] These include for example electron beam evaporation, thermal evaporation, sputtering, and laser ablation. Typically PVD has been used to deposit several inorganic materials including oxides[59], nitrides[60], carbides[61], and sulphides[62]. Even though PVD methods produce films with good thermal and mechanical stability, the downside is line-of-sight deposition. Coating complex objects with varying morphology would require rotating the object or placing several source material targets around it.

The main challenge in depositing inorganic–organic hybrid thin films by PVD methods is decomposition of the organic constituents in the source material. This usually rules out PVD techniques with high energy beams such as electron beam evaporation and laser ablation. However, some examples of hybrid PVD exist. Xiao *et al.* used thermal evaporation to deposit free standing metal octaethylporphyrin (MOEP) films.[63] MOEP was heated to 325 °C under nitrogen flow to prevent oxidation and the film was deposited on an ionic liquid surface. In another study Bonomi *et al.* utilized RF-magnetron sputtering to deposit films of hybrid perovskites.[64] A single target of CH_3NH_3I and PbI_2 mixture was sputtered with argon and the films were deposited on quartz substrates. Highly crystalline $CH_3NH_3PbI_3$ films with a low PbI_2 impurity content and full substrate coverage were obtained by optimizing the gas pressure, RF-power, and target to substrate distance.

2.3.2.2 Chemical Vapor Deposition

In CVD evaporated precursors or gases are led onto a substrate where they react and/or decompose to form a film. The process results in volatile byproducts which are removed by flowing inert gas.[65] There are several variations of CVD, which can be classified by the operating conditions. For example the deposition can be done under atmospheric pressure (APCVD), low pressure (LPCVD) or ultrahigh vacuum (UHCVD). Also the driving force for the chemical reactions and decomposition of the precursors can be different. These variations include thermal CVD, plasma enhanced CVD (PECVD), laser CVD, and photo-initiated CVD. Also ALD and MLD

are variations of CVD, but often referred to as separate methods due to their unique characteristics discussed in Chapters 2.1 and 2.2. Compared to PVD, the great advantage of CVD is that it enables coating of complex 3D objects.

One of the most important aspects in CVD processes is choosing the precursors. Besides reactivity and evaporation temperature, one also needs to consider price and toxicity especially when it comes to large scale industrial use. In particular finding the right organic precursors for the CVD of inorganic–organic hybrid films can be demanding as decomposition must be avoided, and the functional groups must react readily with the inorganic precursor to form the desired bonds in the gas phase or on the surface.

Especially PECVD has been used to deposit inorganic–organic hybrid films. Cho *et al*. used tetraethylorthosilane and cyclohexene to deposit low-k films by PECVD and studied the effects of plasma power and mixing ratio of the precursors on the film properties.[66] Dielectric constant as low as 2.7 was achieved and the growth rate and dielectric constant were tunable by changing the plasma power and precursor ratio. Even lower dielectric constant of 1.6 was reported by Seo et al. for films deposited by the same process.[67] This was achieved by varying the tetraethylorthosilane flux. PECVD was used also by Li *et al*. to prepare inorganic–organic permeation barriers for solar cells.[68] A mixture of hexamethyldisiloxane and O_2 was used as the precursor at room temperature. The ratio of the inorganic and organic constituents in the films could be controlled by changing the plasma power and precursor mixing ratio. This was observed to have a direct relation to the permeation properties, and with optimized parameters a water vapor transmission rate as low as 3.6×10^{-6} g m^{-2} day^{-1} was achieved with a 1.5 µm thick film.

2.3.2.3 Atomic and Molecular Layer Deposition

As discussed in Chapters 2.1 and 2.2, ALD and MLD are variations of the conventional CVD. The main difference is that in ALD/MLD precursors react in a surface controlled manner (Figure 1) through self-limiting reactions and ideally no decomposition occurs. This makes ALD/MLD a convenient tool for depositing inorganic–organic hybrid materials as it allows mixing the constituents in a controlled way. In addition, by varying the cycling ratios of inorganic ALD and organic MLD, the film properties can be tuned at molecular level. While MLD of polymers was realized for the first time already in the beginning of the 1990's,[12] the first studies on combining ALD and MLD to deposit inorganic–organic hybrid films were published around 2007.[69] During the last decade a vast selection of different precursor combinations have been used and some of them are listed in Table 1. Some pioneering work on ALD/MLD hybrids will be discussed more closely in the following chapters.

Table 1. Common precursors used in ALD/MLD of hybrid thin films.

Metal precursor	Organic Precursors	Ref
TMA	Ethylene glycol	70
	Suberic acid	75,76
	Succinic acid	75,76
	1,2-benzenedicarboxylic acid	74
	1,3-benzenedicarboxylic acid	74,76
	1,3,5-benzenetricarboxylic acid	74
	1,2,4,5-benzenetetracarboxylic acid	74,76
	(2E,4E)-hexa-2,4-dienedioic acid	74
	(E)-butenedioic acid	74
	(Z)-butenedioic acid	74
	Heptanedioic acid	74
	Octanedioic acid	74
	Ethanedioic acid	74
	Decanedioic acid	74
	Pentanedioic acid	74
	Propanedioic acid	74
	8-hydroxyquinoline	74,78
	Hydroquinone	74
	1,3,5-benzenetriol	74
	Oxiran-2-ylmethanol	81
DEZ	Ethylene glycol	71
	8-hydroxyquinoline	74
	4-aminophenol	79
$TiCl_4$	8-hydroxyquinoline	74
	Ethylenediamine	74
	4-aminophenol	80
	4-aminobenzoic acid	74
$M(thd)_x$ (M = Ca, Co, Cu, Eu, Li, Mn)	1,4-benzenedicarboxylic acid	82–84,89
	3,5-pyridinedicarboxylic acid	88,89
	2,6-pyridinedicarboxylic acid	89
$ZrCl_4$	Ethylene glycol	72
	1,4-benzenedicarboxylic acid	95
	2-amino-1,4-benzenedicarboxylic acid	96
$HfCl_4$	Ethylene glycol	71
$Ti(OPr)_4$	7-octanyltrichlorosilane	69

A good example of combining inorganic and organic constituents by ALD/MLD to obtain novel material properties was first shown in 2007 by Lee *et al.*[69] Titanium isopropoxide and 7-octynyltrichlorosilane were used together with ozone and H_2O to deposit hybrid multilayers with tunable electrical properties. ALD/MLD enabled an easy control of layer thicknesses and provided sharp interfaces (Figure 8). Also the electrical stability of the films was improved compared to bare TiO_2.

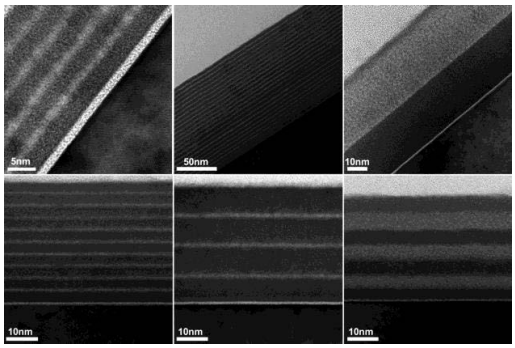

Figure 8. TEM images of TiO_2/7-OTS multilayers deposited by ALD/MLD. Reprinted from Ref. 69, with permission from ACS Publications.

Another early approach to deposit hybrid thin films by ALD/MLD used metal alkyls with diols. Dameron *et al*. deposited so called alucone films using trimethylaluminum (TMA) and ethylene glycol (EG) as the precursors.[70] Although the growth was shown to be saturative and self-limiting, it was interestingly observed that TMA molecules can be absorbed inside the film and react from there with EG during the subsequent pulses. Infrared spectroscopy also revealed that EG can go through a double reaction from its both ends because of the excess TMA stored inside the film. Analogous to the alucones, zincones were deposited using diethyl zinc (DEZ) and EG.[71] The growth characteristics were very similar to the alucone deposition, and the double reaction of EG was found to be an important part of the reaction mechanism. Both the alucone and zincone films were unstable in air. In the case of zincones it was interestingly observed that hydrolysis of the hybrid films results in ZnO films with nanoscale porosity throughout the material. Later on Lee *et al.* have used the same approach to deposit zircones[72] and hafnicones[73].

Nilsen and coworkers have explored a good compilation of ALD/MLD hybrid processes using TMA, DEZ, and titanium tetrachloride ($TiCl_4$) as the inorganic precursor and various alcohols, carboxylic acids, and amines as the organic precursors.[74,75] It was concluded that a vast collection of different organic molecules can be utilized for depositing inorganic–organic hybrid thin films in a self-limiting manner. Selection of the organic backbone seems to be of great importance as larger molecules

can cause steric hindrance inhibiting the growth. On the other hand, linear molecules can undergo double reactions similar to those already seen in the case of alucones[70] and zincones[71]. This can cause unforeseen variation in the growth or inhibit the growth completely. While hybrid films deposited using alcohols and amines tend to react with air over long exposure times, it was found out that using carboxylic acids produces more stable films.[74] Another interesting finding was that aluminates deposited with TMA and linear carboxylic acids may exhibit low leakage currents and dielectric constants as low as 2.5.[76]

TMA, DEZ, and $TiCl_4$ have also been used as precursors with 8-hydroxyquinoline to deposit metal quinoline (Mq_x) films.[74,77] While the conventional ALD/MLD processes deposit films with covalently bonded polymeric structures, metal quinolines are held together by van der Waals interactions. It was shown that ALD/MLD is a potential method for depositing Alq_3 and Znq_2 films, which have applications as photoluminescent materials in OLED displays.[78] As the film growth occurs through chemisorption and adsorption, all the Mq_x processes were strongly dependent on the deposition temperature.

To avoid unpredictable growth due to the double reactions, heterobifunctional molecules have been studied as the organic precursor. One such example is 4-aminophenol used together with DEZ by Sood *et al.*[79] Interestingly, a temperature window of constant growth rate was observed in the range of 140–200 °C which is uncommon for MLD processes. Similar results were also reported by Sundberg *et al*. for a process using $TiCl_4$ and 4-aminophenol, though the range of the constant growth rate was narrower at 140–160 °C.[80] The heterobifunctionality can also be achieved by using cyclic molecules that undergo a ring opening reaction during the deposition. One of the first examples of such a strategy was presented by Gong *et al*.[81] They used TMA with oxiran-2-ylmethanol and showed that Al can catalyze an epoxy ring opening reaction after oxiran-2-ylmethanol has reacted with the Al-CH_3 surface (Figure 9). While it was concluded that oxiran-2-ylmethanol reacts with the surface from its both ends during the exposure, the ring opening reaction leaves hydroxyl groups on the surface, which can react with TMA during the next step. It was also noted that subsurface diffusion of TMA increases the growth rate especially in

the case of thicker films. The films were found to be relatively stable at ambient conditions, and post-deposition annealing in air produced well-defined porous inorganic structures.

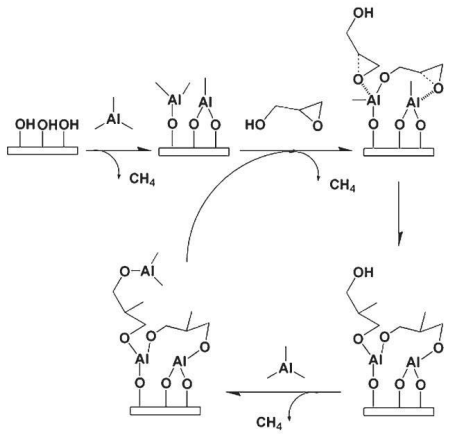

Figure 9. Schematic illustration of the surface reactions during TMA/oxiran-2-ylmethanol MLD process. Reprinted from Ref. 81, with permission from ACS Publications.

While most of the inorganic–organic hybrid thin films are amorphous as-deposited, some processes using 1,4-benzenedicarboxylic acid yield crystalline films. The largest motivation for searching precursors and growth conditions to obtain crystalline hybrid films by ALD/MLD has arisen from MOFs. The porosity of these materials is extraordinary, and the ability to deposit them by ALD/MLD would open up many new applications. The first as-deposited crystalline ALD/MLD films were reported by Ahvenniemi *et al*. who deposited copper(II)terephthalate films using copper 2,2,6,6-tetramethyl-3,5-heptanedione ($Cu(thd)_2$) and 1,4-benzenedicarboxylic acid as the precursors.[82] Crystalline films were obtained only at the deposition temperature of 180 °C, and X-ray diffraction confirmed a paddle-wheel-type MOF-2 structure. Since then, ALD/MLD made lithium and calcium terephthalate films have been reported to have crystalline structures as-deposited.[83,84] The intrinsic porosity of these materials is so low that they are usually classified as coordination polymers instead of MOFs, but they have other promising applications such as battery cathodes[85,86]. Several other ALD/MLD processes using $M(thd)_x$ (M

= Co, Eu, Mn) compounds and various dicarboxylic acids as the precursors have been reported in the literature but these films exhibit no crystallinity.[87–89]

2.3.2.4 Post-Deposition Conversion

Direct vapor phase deposition is not feasible for all hybrid materials. The problem can be the availability of suitable precursors or the resulting material does not have desired properties as-deposited. However, in some cases it is possible to do post-deposition conversions in gas or liquid phase. The challenging part in using these conversion methods is to find the right conversion parameters. In liquid conversion, for example, the solvent, reactants, temperature, and treatment time are of utmost importance for achieving complete conversion without undesired effects such as dissolution of the film.

ZIF-8 is a zeolitic imidazolate framework consisting of zinc ions connected with 2-methylimidazole linkers. It has good mechanical properties and a dielectric constant below 2.5, which makes ZIF-8 a potential low-k candidate for microelectronic applications.[90] One approach to make ZIF-8 films has been the conversion reaction of ZnO with 2-methylimidazole. This was first realized by Khaletskaya et al. in liquid phase using sputtered and ALD ZnO films.[91] The gas phase conversion of ALD ZnO into ZIF-8 was demonstrated by Stassen *et al*.[92] ALD of ZnO was conducted using diethyl zinc and H_2O as the precursors followed by a conversion to ZIF-8 using 2-methylimidazole vapor in a closed reactor vessel. It was shown that conformal ZIF-8 films could be deposited even onto high aspect ratio features (Figure 10).

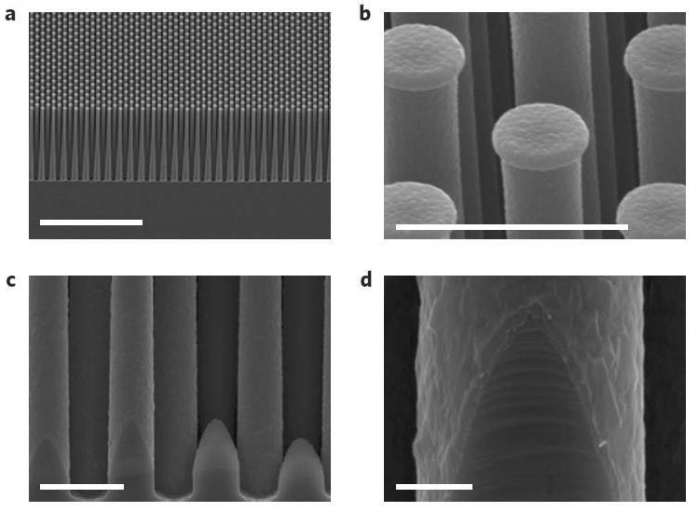

Figure 10. ZIF-8 films deposited on a high aspect ratio silicon pillar array by ALD of ZnO and a conversion reaction (a and b). The ZIF-8 film was homogeneous also at the base of the pillars (c and d). Reprinted from Ref. 92, with permission from Springer Nature Limited.

In later studies Krishtap *et al*. showed that expansion of the film during the gas phase conversion of ZnO to ZIF-8 can be exploited in filling gaps between inter-connect lines of integrated circuits.[93] Furthermore, the gas phase ZIF-8 conversion process has been upscaled on 200 mm Si wafers in cleanroom conditions by Cruz *et al*.[94] This demonstrates that conversion reactions provide a realistic way for integrating MOFs into thin film devices for industrial applications.

Lausund et al. have used a conversion of MLD zirconium terephthalate films to form UiO-66 MOF films.[95] In this case $ZrCl_4$ and 1,4-benzenedicarboxylic acid were used as the precursors to deposit hybrid thin films. Normally the process yields amorphous films that cannot be crystallized afterwards. However, pulsing acetic acid after each reaction cycle to control the coordination state of 1,4-carboxylic acid was found to enable post-deposition crystallization of the material into UiO-66. The crystallization was done in an autoclave with acetic acid vapor. The films were found to be continuous and their crystal structure matched with UiO-66. Later it has been found out that the acetic acid modulation can be excluded

by using 2-amino-1,4-benzenedicarboxylic acid.[96] The amino group creates steric hindrance and thereby ensures that the linkers coordinate only in the bidentate manner.

The main problem with the post-deposition conversion methods is that only films of certain thicknesses can be fully converted because the conversion product covers the original film and thereby slows down the reaction. For example in the case of gas phase conversion of ZnO to ZIF-8, it was reported that only up to 15 nm thick ZnO films were fully converted.[92] Liquid phase conversion methods can also have limits in the conformality on high aspect ratio features.

3. Experimental

3.1 Film Deposition

All films were deposited in a hot-wall, flow-type ASM Microchemistry F-120 ALD reactor.[I–IV] Nitrogen (99.999%, Labgas NG 2) was used as the carrier and purging gas and the pressure inside the reactor was ~7 mbar. The flat substrates were silicon (100)[I–IV] and ITO films on glass[I]. For conformality studies trenched Si was used.[II,III] For catalytic testing samples of zinc glutarate (ZnGA) were deposited on steel mesh and glass wool.[IV] All the precursors used in this thesis and their evaporation temperatures, suppliers, and purities are listed in Table 2. Water was pulsed into the reactor from an external source through a needle valve at room temperature.[I]

Table 2. All the precursors used in this thesis.

Precursor	Evaporation T (°C)	Supplier, Purity
Tantalum ethoxide ($Ta(OEt)_5$)[I]	100	Epichem, N/A
Pyromellitic dianhydride (PMDA)[I]	150	Aldrich, 97%
Diaminohexane (DAH)[I]	40	Fluka, ≥99%)
Zinc acetate ($ZnAc_2$)[II–IV]	190	Merck, 99.5%
1,4-benzenedicarboxylic (1,4-BDC)[II]	220	Aldrich, >99%
2,6-naphthalenedicarboxylic acid (2,6-NDC)[III]	250	Aldrich, 99%
Glutaric acid (GA)[IV]	100	Aldrich, 99%

The initial crystallization of the MOF thin films was carried out in a humidity-controlled box at a relative humidity of 60–80%.[II,III] Parr 4744 general-purpose acid digestion bomb was used to recrystallize the films in DMF (Lab-Scan, 99.8%) into the desired phase.[II,III]

3.2 Characterization Methods

Hitachi U2000 spectrophotometer and a fitting program by Ylilammi and Rantaaho[97] were used to analyze thicknesses and refractive indices of the films.[I–IV] The thicknesses of the thinnest layers were determined from X-ray reflection (XRR) patterns measured with a PANalytical X'Pert Pro MPD diffractometer.[I] Optical images were taken with an Olympus PX51 light microscope[II–IV] and field emission scanning electron microscopy (FESEM) images with a Hitachi S-4800 FESEM[I–IV]. Energy-dispersive X-ray spectroscopy (EDS) measurements of ZnGA films were performed in the Hitachi S-4800 FESEM equipped with an Oxford Instrument Inca 350 EDS system.[IV]

Electrical properties were measured from Al/film/ITO capacitor structures on glass substrates using a HP 4284A precision LCR meter and a Keithley 2400 SourceMeter.[I] The Al electrodes were electron beam evaporated through a shadow mask with a dot size of 2.04×10^{-3} cm^2.

Crystallinity of the films was studied with X-ray diffraction (XRD) using a PANalytical X'Pert Pro MPD diffractometer.[II–IV] High-temperature X-ray diffraction (HTXRD) was carried out in an Anton Paar HTK-1200N oven-chamber attached to the diffractometer.[II,III] The measurements were done in air and N_2 (99.999%, Entegris 35KF-I-4R purifier, Aga).

Composition of the films was studied with Fourier transform infrared spectroscopy (FTIR)[II–IV] and time-of-flight elastic recoil detection analysis (TOF-ERDA)[II,III]. FTIR measurements were carried out with a PerkinElmer Spectrum GX FTIR system on silicon substrates in a transmission mode. The TOF-ERDA analyses were done using 8.52 MeV $^{35}Cl^{5+}$ ions from a 1.7 MV Pelletron accelerator.

Atomic force microscopy (AFM) images were recorded with a Veeco Multimode V instrument operated in a tapping mode in air using silicon probes with a nominal tip radius of 10 nm and a nominal spring constant of 3 Nm^{-1} (VLFM from Bruker).[I,IV]

AFM based qualitative nanoindentations were made with a diamond-tipped probe delivered by Bruker.[I–III]

Porosity measurements were done with a UV-Vis (λ = 240–1000 nm) variable angle spectroscopic ellipsometer (Woollam VASE – 2000U).[II] Environmental ellipsometry porosimetry was carried out by capillary condensation of isopropanol into the pores using an atmospheric control chamber designed by SOPRA-LAB(X).

Vapor phase loading of the IRMOF-8 films with $Pd(thd)_2$ (thd=2,2,6,6-tetramethyl-3,5-heptanedionato, ABCR 98%) was carried out in a Schlenk bottle.[III] A FEI Quanta 3D 200i focused ion beam scanning electron microscope (FIB-SEM) fitted with an Oxford Instrument Inca 350 EDS system was used for cross section lamella lift-out and EDS measurements of the Pd loaded films. A 10 kV electron beam was used for the x-ray mapping.

Nuclear magnetic resonance (NMR) experiments were performed on a Varian Mercury Plus 300 MHz instrument (1H-frequency 300 MHz).[IV] Size-exclusion chromatography (SEC) analysis of the polymer was performed using a Waters ACQUITY APC system equipped with an IR-detector.[IV]

4. Results and Discussion

The main results of this thesis are summarized in this chapter. A more detailed description of the processes and characteristics of the films can be found in publications I–IV.

4.1 ALD of Ta_2O_5/Polyimide Nanolaminates

Layering distinct materials as nanolaminates is a well-known method for tailoring film properties. The ability to deposit conformal films with a good control over film thickness makes ALD an ideal method for making nanolaminates with sharp interfaces. There are several examples of inorganic ALD nanolaminates where desired dielectric, thermal, and mechanical properties have been achieved by optimizing the individual layer thicknesses.[7,98–100] Also the combination of ALD and MLD has been used to deposit inorganic–organic multilayers.[101,102] While nanolaminates are usually classified as composites, inorganic–organic nanolaminates with individual layer thicknesses from some Ångtröms to a few nanometers can be considered hybrid materials.

An ALD process using $Ta(OEt)_5/H_2O$ and an MLD process using PMDA/DAH as the precursors were combined to deposit Ta_2O_5/polyimide nanolaminates.[103,13,I] Particularly the effects of the bilayer thicknesses on dielectric and mechanical properties were investigated.

4.1.1 Film Growth

The growth behavior of Ta_2O_5 and polyimide on each other was studied by depositing single bilayers at 170 °C. The deposition temperature was set as high as possible to obtain Ta_2O_5 with as low impurity content as possible while keeping in mind that the polyimide growth is strongly temperature dependent and stops at 200 °C.[13] The

growth rate of Ta_2O_5 on polyimide did not differ significantly from that on a Si substrate while the polyimide growth rate was 0.5 Å/cycle lower on Ta_2O_5 (5.6 vs. 5.1 Å/cycle). Six nanolaminates with different target thicknesses were finally deposited for characterization (Table 3). XRR studies of the nanolaminates showed that the actual thicknesses of the individual layers were lower than targeted. This could indicate that the start of the growth is delayed when Ta_2O_5 and polyimide are deposited on each other. However, the nanolaminates consisted of distinct layers with relatively sharp interfaces (Figure 11).

Table 3. Ta_2O_5/polyimide nanolaminate target structures.

Target Structure
5 × (15 nm PI + 5nm Ta_2O_5)/substrate
5 × (10 nm PI + 10nm Ta_2O_5)/substrate
5 × (5nm PI + 15nm Ta_2O_5)/substrate
5 × (15 nm Ta_2O_5 + 5 nm PI)/substrate
5 × (10 nm Ta_2O_5 + 10nm PI)/substrate
5 × (5nm Ta_2O_5 + 15nm PI)/substrate

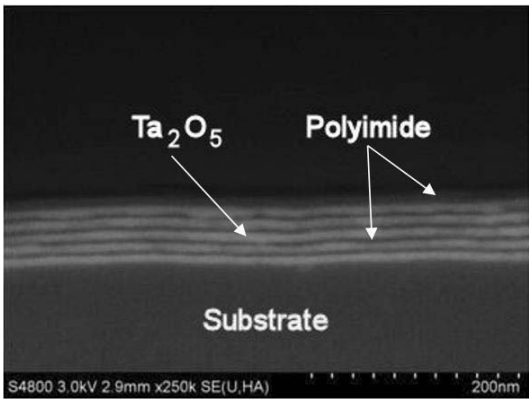

Figure 11. Cross-sectional FESEM image of the nanolaminate with 10 + 10 nm bilayers.[I]

4.1.2 Dielectric Properties

Kukli et al. have shown that laminating inorganic materials is a very effective way for reducing leakage currents.[7] Similar behavior was seen also with the Ta_2O_5/polyimide nanolaminates. While relatively high leakage currents of 5×10^{-4} and 4×10^{-5} A/cm^2 at 1 MV cm^{-1} were measured for the bare Ta_2O_5 and polyimide films, about ~30-fold decrease was observed for the nanolaminate with 15 nm polyimide and 5 nm Ta_2O_5 layers. This can be attributed to the elimination of leakage inducing through-insulator defects by laminating of the materials; in the nanolaminates with five bilayers there are nine internal interfaces between polyimide and Ta_2O_5. Overall the general trend was that increasing the Ta_2O_5 content increased the leakage current (Figure 12), which was expected as bare Ta_2O_5 is known to have high leakage[103].

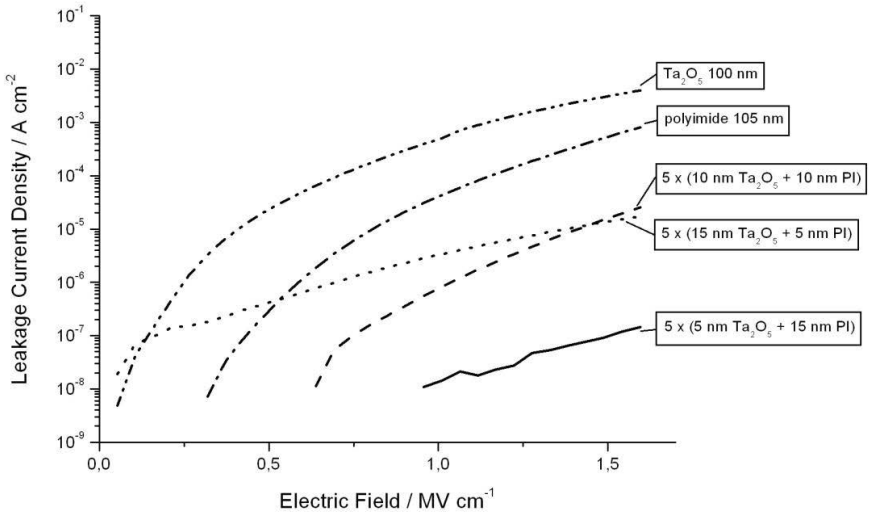

Figure 12. Leakage currents of bare Ta_2O_5 and polyimide films and selected nanolaminates.[I]

The measured permittivities of 20 and 3 for Ta_2O_5 and polyimide were close to the values reported earlier in the literature.[103,104] While the bare films showed unstable *C-V* behavior, the nanolaminates had low voltage dependence with only little hysteresis. However, surprisingly the dependence of the permittivity on the Ta_2O_5 content was not linear. It seems that polyimide is more dominant in a way that the permittivities of the nanolaminates were much lower than expected (Figure 13). This is a good example of unexpected results when combining inorganic and organic constituents at nanoscale.

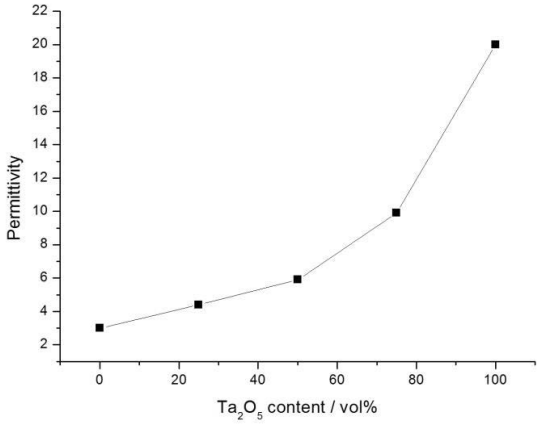

Figure 13. Permittivities of the Ta_2O_5/polyimide nanolaminates relative to the Ta_2O_5 content.

4.1.3 Mechanical Properties

AFM based nanoindentation was used to study the mechanical properties of the nanolaminates. Only qualitative measurements were done as comparing the elastic modulus and hardness values to bulk materials would have been vague at best due to the effect of the small film thickness and equipment used. A simple test of indenting ~100 nm thick Ta_2O_5, polyimide and nanolaminate (10 + 10 nm bilayers) films with the same indenter peak loads gave a clear indication that while polyimide is much softer than Ta_2O_5, the laminate is harder than the bare polyimide (Figure 14).

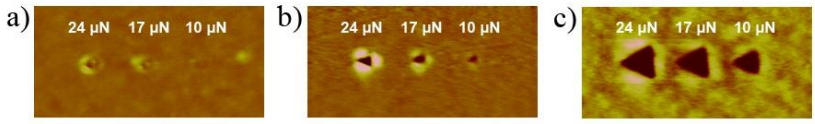

Figure 14. AFM images of indents on a) Ta_2O_5, b) 5 × (10 + 10 nm) nanolaminate, and c) polyimide.

To study further the mechanical characteristics, load vs. displacement curves were measured for the bare films and nanolaminates. The maximum displacement h_{max} correlates with the softness of the material, the recovery during unloading ($h_{max} - h_f$) with the elasticity, and the area between the curves with the plastic deformation. From Figure 15 it can be clearly seen that all these attributes increase with the polyimide content as expected.

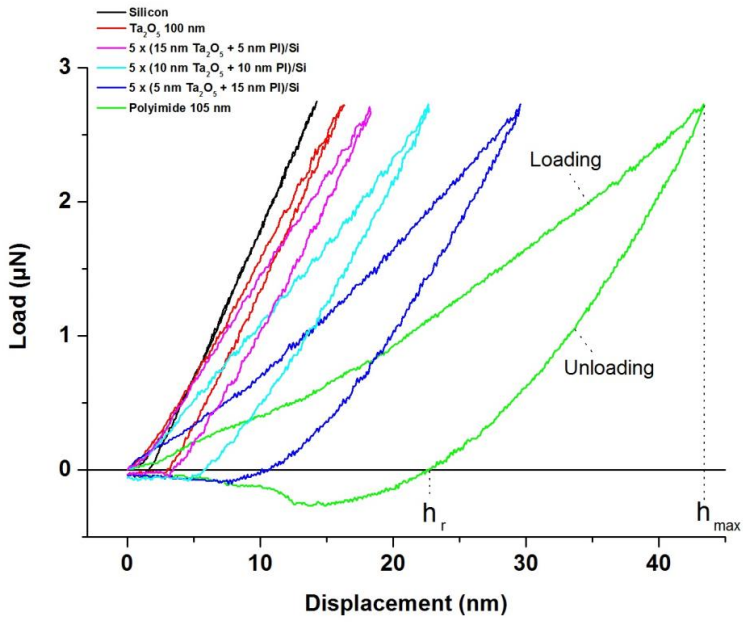

Figure 15. Load vs. displacement curves for the bare Ta_2O_5 and polyimide films and different laminate structures.

4.2 ALD of MOF-5 and IRMOF-8 Thin Films

In the recent years MOFs have been under intensive study for their remarkable porosity. Most of the research has concentrated on powder synthesis, but also thin films have drawn attention. The most convenient way of synthesizing MOFs is to mix the precursors in solution and induce the crystal growth by thermal energy or for example by microwaves. This has been also the starting point for thin film deposition. However, for utilizing MOF films in more advanced applications, such as microelectronics and optics, more sophisticated methods are required to deposit films with good continuity and control over thickness and conformality.

The possibility to deposit MOF thin films by ALD was studied using zinc acetate ($ZnAc_2$) as the metal precursor and 1,4-benzenedicarboxylic acid (1,4-BDC) and 2,6-naphthalenedicarboxylic acid (2,6-NDC) as the linker molecules (Figure 16).[II,III] In addition to the basic growth characteristics and composition, the films were examined for their crystallinity and ability to uptake guest molecules. Furthermore, mechanical properties were examined by nanoindentation.

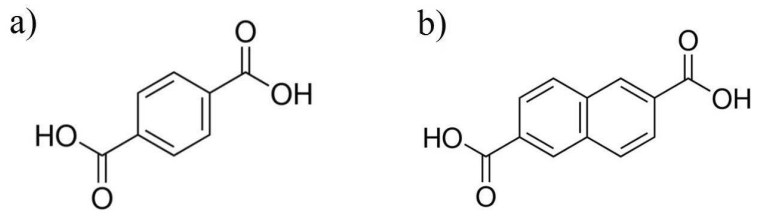

Figure 16. Chemical structure of a) 1,4-benzenedicarboxylic acid and b) 2,6-naphthalenedicarboxylic acid.

4.2.1 Film Growth

$ZnAc_2$ was used as the metal precursor due to its tendency to form Zn_4O clusters[105] which are the inorganic building blocks of MOF-5 and IRMOF-8. Deposition temperature range of 225–350 °C was studied. No growth was observed for the $ZnAc_2$/1,4-BDC process at 350 °C, and visual patterns indicating non-uniform growth started appearing on the films above 300 °C for the $ZnAc_2$/2,6-NDC process. The growth characteristics were explored further at 250 and 260 °C to avoid condensation of 1,4-BDC and 2,6-NDC, evaporated at 220 and 250 °C, while maintaining as high growth rate as possible. Both processes using 1,4-BDC or 2,6-NDC exhibited ALD type of growth with saturating growth rate with increasing pulse lengths (Figure 17) and good control over films thickness by varying the number of deposition cycles. No temperature window of constant growth rate was observed as the growth rates had descending trends with temperature.

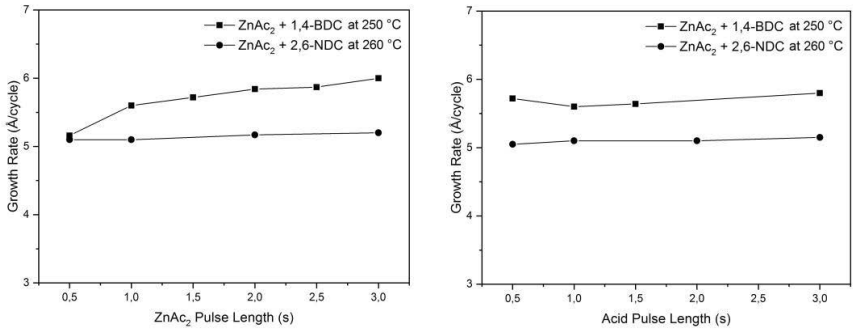

Figure 17. The effect of pulse lengths on growth rates.

4.2.2 Crystallization Studies

All the films were amorphous as-deposited regardless of the deposition temperature. While in most studies on inorganic–organic hybrid thin films it has been reported that the films deposited with carboxylic acids are relatively stable against moisture,[74,75] it was found out that the films studied in this work actually crystallized under 60–70 RH% at room temperature. The large crystallites were visible even with

bare eye and optical microscope (Figure 18). Furthermore, the crystallized phases were stable when kept under the moist conditions for a prolonged time, which is a total opposite of the known tendency of MOF-5 to decompose at over 45 RH%.[106] To test the effect of the metal precursor on the film crystallization, diethyl zinc (DEZ) was used as an alternative metal precursor with 1,4-BDC to deposit films. Identical behavior in humid conditions was observed also with these films indicating that the formation of the Zn_4O cluster from $ZnAc_2$ has no effect on the crystallization.

Figure 18. Optical microscope image of a humidity crystallized film deposited with $ZnAc_2$ and 1,4-BDC.

Grazing incidence XRD (GIXRD) measurements showed that while the crystallized film gave reflections at low 2θ values indicating large unit cells (Figure 19), they were not matching the targeted MOFs. It was interestingly observed that both materials exhibited reversible peak shifts in HTXRD when heated and exposed to moist air again. This suggests that the films can absorb and desorb moisture.

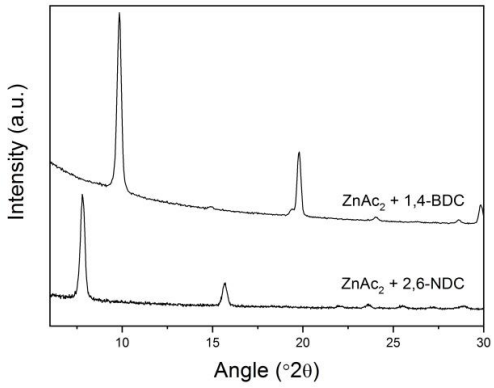

Figure 19. GIXRD diffractograms of the films crystallized in moist air.

Dimethylformamide (DMF) is often used as the solvent in MOF synthesis.[33] Thus, the conversion of the moisture crystallized films in this work was carried out in an autoclave with DMF. A 120 minute treatment at 150 °C was enough for both materials to re-crystallize them into the targeted MOF structures (Figure 20). Unlike the moisture crystallized films, the recrystallized films did not show any structural changes in HTXRD until decomposition to ZnO which was expected based on the earlier studies on MOF-5 and IRMOF-8.[41,107]

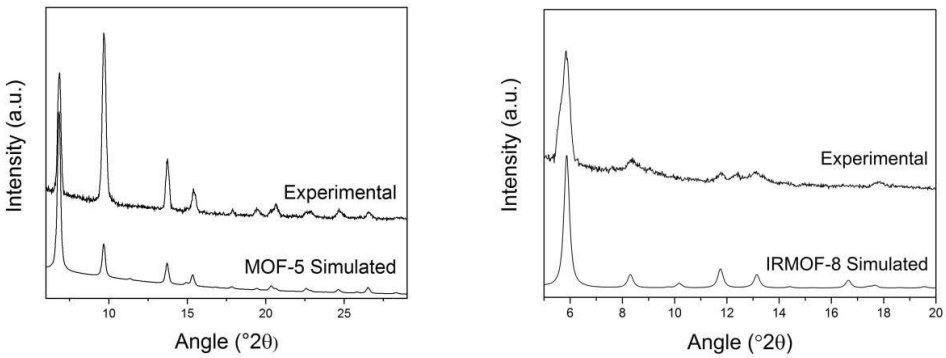

Figure 20. GIXRD diffractograms of the films re-crystallized in DMF.

As poor continuity is often a problem in the synthesis of MOF thin films[41], FESEM was used to study the films re-crystallized in DMF. Unfortunately it was observed that the continuity was lost also in this case (Figure 21 a and b), which is probably due to a partial dissolution in DMF. However, repeating the film deposition and crystallization in DMF improved the continuity greatly (Figure 21 c and d). Even more importantly, it was observed that conformality of the films was preserved in trenches (Figure 22), meaning that the advantage of using ALD was not lost even after the post-deposition crystallization steps.

Porosity of the MOF-5 films was confirmed by measuring the change in refractive index during isopropanol adsorption using spectroscopic ellipsometry. While the high roughness of the films made it impossible to determine the actual pore size, the change in refractive index of the material indicated two clear uptake regions. The uptake was fully reversible upon heating. In the case of IRMOF-8, the ability to up-

take guest molecules was studied by using a volatile palladium compound $Pd(thd)_2$. The IRMOF-8 film was heated under vacuum together with $Pd(thd)_2$ at 120 °C for 24 h to load the $Pd(thd)_2$ molecules into the pores. $Pd(thd)_2$ was then decomposed to metallic palladium by increasing the temperature to 200 °C. The successful loading was confirmed by an immediate color change of the film from white to black. Cross-sectional EDS mapping showed that palladium was uniformly spread throughout the film thickness, thereby verifying that the films were through-porous.

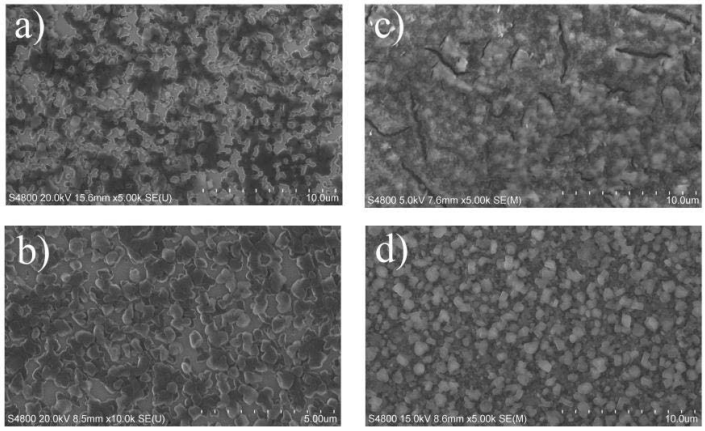

Figure 21. FESEM images of a) MOF-5 crystallized in DMF, b) IRMOF-8 crystallized in DMF, c) MOF-5 after second deposition and crystallization, and d) IRMOF-8 after second deposition and crystallization.

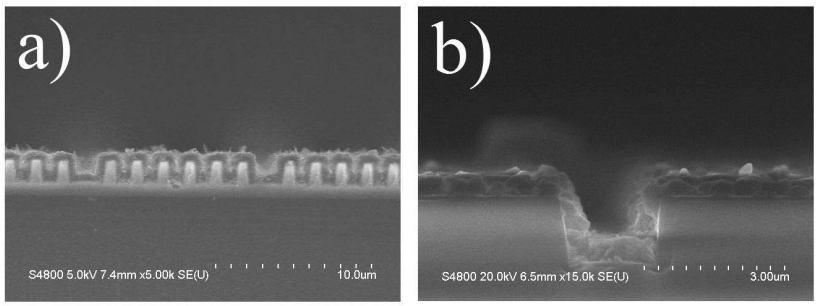

Figure 22. FESEM images of a) MOF-5 and b) IRMOF-8 films deposited on a Si substrate with trenches.

4.2.3 Film Composition and Mechanical Properties

TOF-ERDA analysis of the moisture converted films showed that even though the crystal structures did not match with MOF-5 or IRMOF-8, the compositions were very close (Figure 23 a and b). Because of the high roughness and porosity of the MOF-5 and IRMOF-8 films, compositional analysis of the re-crystallized films could not be done by TOF-ERDA. Instead FTIR was used. As expected, strong signals from COO stretching vibrations were observed as well as weaker bands from Zn-O stretching, which are in line with the earlier reports on MOF-5 and IRMOF-8.[107,108]

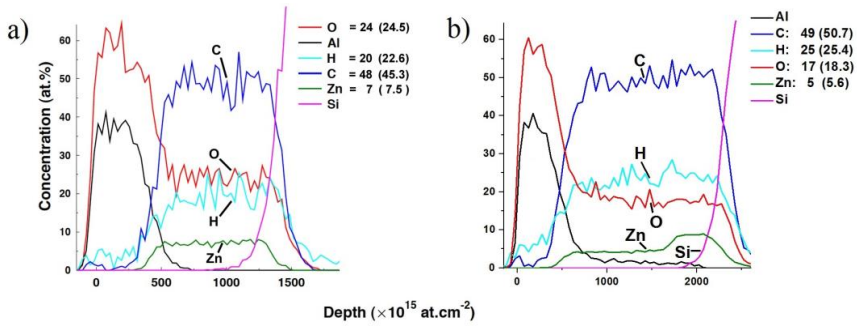

Figure 23. TOF-ERDA results of moisture crystallized films deposited using a) $ZnAc_2$ and 1,4-BDC and b) $ZnAc_2$ and 2,6-NDC. Expected concentrations for MOF-5 and IRMOF-8 are shown in the parenthesis. The films were capped with a protective Al_2O_3 layer to prevent decomposition during the measurement.

While the MOF-5 and IRMOF-8 films were too rough also for the AFM based nanoindentation, mechanical properties of the amorphous and moisture crystallized films were compared to ALD ZnO films. As expected, the organic constituents make the films more elastic and softer than ZnO (Figure 24). It seems that the crystallization does not affect these properties much, although the amorphous as-deposited films seem to be slightly softer.

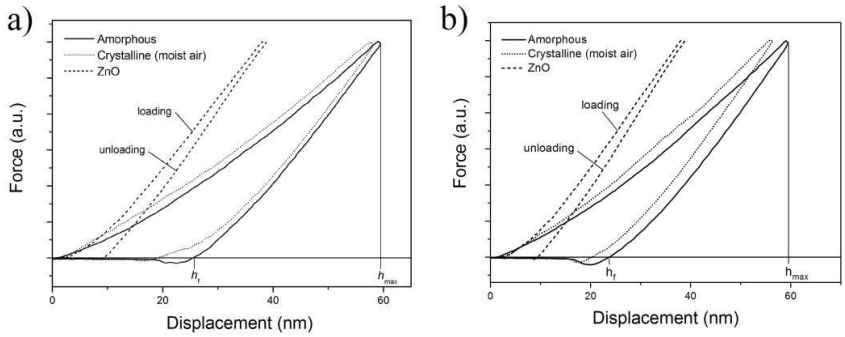

Figure 24. Nanoindentation curves of a ZnO film and the films deposited using a) $ZnAc_2$ and 1,4-BDC and b) $ZnAc_2$ and 2,6-NDC.

4.3 ALD of Zinc Glutarate Thin Films

Zinc glutarate (ZnGA) is a common catalyst used in commercial production of polycarbonates by copolymerization of epoxides and CO_2. It is a coordination compound similar to MOFs and consists of Zn_4O clusters connected by glutarate ligands.[109,110] However, the intrinsic porosity is not large enough to accommodate larger molecules. The catalytic reactions of epoxides and CO_2 occur only on the surface of ZnGA, and therefore increasing the surface area and preventing agglomeration during the polymerization is very important for the catalytic activity.

The possibility to deposit ZnGA by ALD was studied using $ZnAc_2$ and glutaric acid (GA) as the precursors.[IV] While no earlier reports on ZnGA thin films exist, coating of high surface-area substrates could open a new way of making efficient and reusable catalysts for the polycarbonate production.

4.3.1 Film Growth

$ZnAc_2$ was chosen as the zinc precursor because of the good results obtained in the previous experiments with dicarboxylic acids.[II,III] The deposition experiments were

started at 200 °C as limited by the $ZnAc_2$ evaporation temperature and it was quickly found out that increasing the deposition temperature to 225 °C caused visible nonuniformity. However, the films deposited at 200 °C were crystalline as-deposited with a structure matching to ZnGA (further discussed in Chapter 4.3.2). Thus, the growth characterization was carried out at 200 °C.

The first 10 cycles produced no film but after that the growth rate started to increase rapidly indicating a non-ALD type growth mode (Figure 25 a). The increase in film thickness also induced a large increase in surface roughness making the thickness measurements by optical methods impossible after 100 cycles. The thickness of these rough films was measured by EDS. Instead of the actual thickness, the k ratio of Zn, which to a first approximation is proportional to the amount Zn in the films, was followed as a function of the number of deposition cycles. Interestingly it was found out that the process had two growth regions (Figure 25 b). During the first 200 cycles the increase in growth rate is also seen in a rapid increase in the amount of Zn. After this the growth continues at a much lower pace in a more ALD-like mode as seen from the proportionality of the Zn k ratio on the number of deposition cycles.

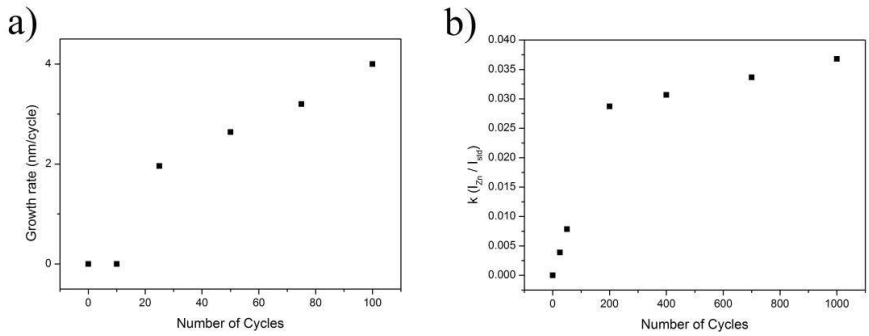

Figure 25. ZnGA growth rate during the first 100 cycles (a) and the amount of zinc in the films, indicated by the EDS k ratio of Zn, as a function of the number of deposition cycles (b).

To gain some further insight to the film growth, the effects of pulse lengths were studied by depositing 50 cycle films. These films were smooth enough to measure

their thicknesses reliably by UV-Vis reflectance spectrometry. The growth rate saturated already with a 1 s GA pulse, but on the contrary no saturation was seen with increasing $ZnAc_2$ pulse length. Interestingly, it was found that the GA purge time has a clear effect on the saturation in respect of the $ZnAc_2$ pulse length (Figure 26). Increasing the GA purge to 6 s resulted in pseudo-saturation with 1–3 s $ZnAc_2$ pulses. With longer pulse times the film thickness started to increase again. This kind of behavior may indicate that the film can actually absorb GA molecules and thereby act as a GA source during the $ZnAc_2$ pulse. Similar effects have been observed in other hybrid MLD processes.[70,71,81] The effect can be minimized with sufficiently long purge times to allow desorption of the absorbed molecules. In the case of ZnGA, the increasing film thickness with $ZnAc_2$ pulses longer than 3 s would suggest that the ZnGA film is porous enough to absorb also $ZnAc_2$ when long enough exposure is used.

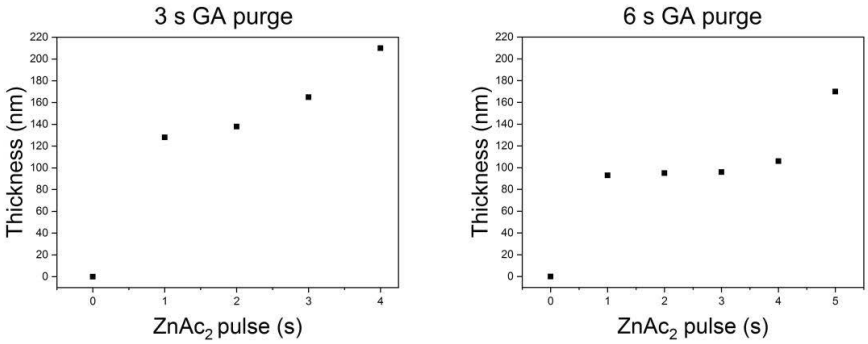

Figure 26. ZnGA film thickness as a function of $ZnAc_2$ pulse length with 3 and 6 s GA purge times.

4.3.2 Film Composition and Morphology

As crystallinity is an important factor in the catalytic activity of ZnGA,[111,112] the films deposited at 200 °C were first characterized by XRD. While there are only a few reports on crystalline inorganic–organic films deposited by ALD/MLD,[82–84] it was surprisingly found out that the films deposited using $ZnAc_2$ and GA were crystalline as-deposited with a structure matching to ZnGA synthesized by other meth-

ods[112,113] (Figure 27). Based on the θ-2θ measurements (Figure 27 b) the films were strongly oriented as only (h00) planes were seen. This is especially true for the thicker 1000 cycle film. In GIXRD measurement the scattering vector tilts away from the surface normal. At small 2θ values the scattering vector is still close to the surface normal, and therefore the likelihood of finding (h00) planes is high. As the scattering vector keeps moving away from the surface normal at higher 2θ values, the intensities of (h00) reflections decrease. This effect is seen in Figure 27 a where the intensity of the (100) reflection is higher than the intensity of the (200) reflection for the 1000 cycle film.

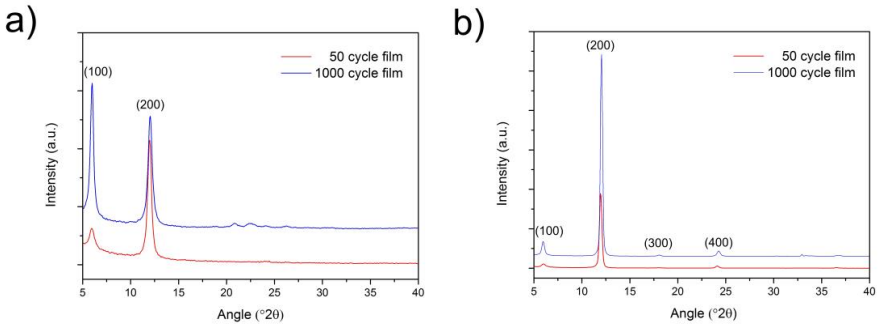

Figure 27. GIXRD (a) and θ-2θ XRD (b) diffractograms of 50 and 1000 ALD cycle ZnGA films.[IV]

AFM revealed that surface morphology of the films with <100 cycles was not very consistent. The 50 cycle film was otherwise smooth (R_q = 1.3–6.4 nm) but deep holes were seen scattered across the film (Figure 28). The rapid change in roughness with increasing film thickness was confirmed by AFM as the film deposited with 200 cycles had large valley-like features with an R_q value of 40 nm (Figure 23).

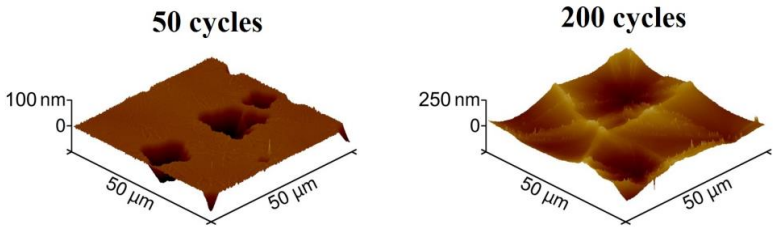

Figure 28. AFM images of ZnGA films deposited with 50 and 200 cycles.

Film composition was studied also by FTIR and TOF-ERDA. The FTIR spectrum was a good match to literature on ZnGA showing vibrations from Zn coordinated carboxylates. Even though the TOF-ERDA measurement was challenging due to sample decomposition under the ion beam, a close match of the elemental contents to the expected ones was observed (Table 4).

Table 4. Elemental contents of a ZnGA film measured by TOF-ERDA.

Element	Measured at.%	Expected at.%
Zn	7.8±1	6.2
C	25.8±3	31.3
H	43.3±5	37.5
O	23.1±2	25.0

4.3.3 Catalytic activity

To study the catalytic activity of the ZnGA films, samples were deposited on steel mesh and glass wool and used as catalysts in copolymerization reactions of propylene oxide and CO_2. FESEM images showed that a homogenous coating of the steel mesh was achieved with 200 cycles (Figure 29). The deep features on the steel mesh were completely filled by the film. According to the AFM and XRD measurements, the 200 cycle films were considered optimal for catalysis based on the surface morphology and crystallinity.

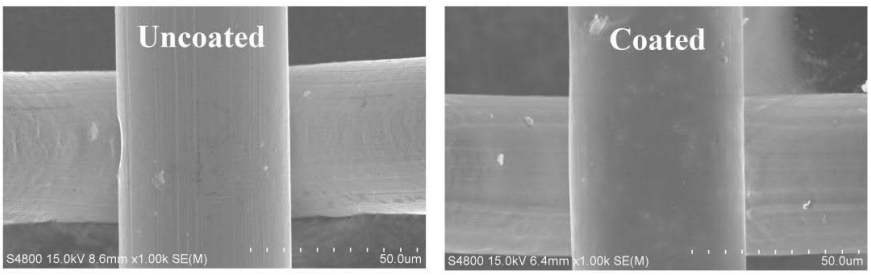

Figure 29. FESEM images of uncoated steel mesh and steel mesh coated with 200 cycles of ZnGA.

10.0 mg of polymer was obtained using 2 ml of propylene and 40 bars of CO_2 regardless of the substrate used in the ZnGA samples. However, according to the ^1H NMR analysis, only 22 % of the polymer was polycarbonate when the glass wool sample was used, and even less, 10 % with the steel mesh sample, the rest being polyether. This was an expected result as the glass wool has clearly higher surface area. The experiment was repeated also without the catalyst and no polymer was obtained.

Size-exclusion chromatography (SEC) was used to study the molecular weights of the polymer samples synthesized with ZnGA on glass wool as the catalyst. The chromatogram showed a peak matching to a molecular weight of 183000 g/mol with polydispersity of 1.041. This indicates that the polymerization proceeded in a controlled way. Another peak was also seen in the oligomeric region (M_n = 1300 g/mol) probably emerging from polymerization reactions that were deactivated at an early stage.

While the results prove that ZnGA deposited by ALD is catalytically active and able to produce polycarbonate with a relatively high molecular weight, comparison to commercial catalysts is quite challenging. This is due to difficulties in determining the actual weight of ZnGA on the substrates and also the limited sizes of ALD and polymerization reactors.

5. Conclusions and Outlook

Since 2007 the field of ALD/MLD research on inorganic–organic hybrid materials has experienced exponential growth. Great number of different organic molecules has been tested with conventional ALD metal precursors such as TMA, DEZ, and $TiCl_4$ to deposit completely new materials. Another objective of these studies has been extending the use of ALD/MLD to known hybrid materials to open up new potential applications. It is known that inorganic–organic hybrid materials can exhibit completely new characteristics not inherent to their constituents. This is also true for many of the deposition processes as the result is not always ideal ALD/MLD. However, as long as the resulting material has desired properties and the advantages of ALD/MLD are not lost, these processes may serve important purposes in the future. In this work the use of ALD/MLD was extended to new types of inorganic–organic hybrid materials including nanolaminates, metal–organic frameworks, and zinc glutarate.

Nanolaminates of polyimide and Ta_2O_5 were deposited using the previously developed ALD and MLD processes. The dielectric properties could be easily tailored by changing the individual layer thicknesses. While the achieved leakage currents and dielectric constants did not exceed the all inorganic nanolaminates reported earlier in the literature, it was shown that the mechanical properties of the films can be greatly improved by the organic constituent. This could be very useful especially in the flexible electronics. While the scope of this study was limited to two materials, it would be interesting to examine more material combinations and test nanolaminates containing also hybrid material layers with organics or inorganics.

Deposition of MOF-5 and IRMOF-8 thin films was studied using $ZnAc_2$, 1,4-BDC, and 2,6-NDC as the precursors. The deposition processes exhibited ALD-like growth characteristics, but the films were amorphous as-deposited. It was discovered that the amorphous films could be crystallized first in moist air and finally in an autoclave in DMF to obtain structures matching with targeted MOFs. Porosity of the films was confirmed by absorption studies and loading guest molecules into the films. Even though the MOF films could not be deposited directly by ALD, it was

shown that the post-deposition crystallized films were conformal and continuous even on trenched substrates. Since 2013 several other reports of similar methodology have appeared in the literature further proving that this kind of post-deposition conversion is a feasible way to various MOF materials in the form of thin films.

ZnGA films were deposited for the first time ever using $ZnAc_2$ and glutaric acid as the precursors. The process was by no means ideal ALD, but still controllable enough to coat 3D substrates conformally with desired film thickness. The films were crystalline as-deposited with a structure matching to ZnGA. Catalytic activity of the films was demonstrated by polymerizing propylene oxide with CO_2 in the presence of the ZnGA coated substrates. The study was severely limited by the size of the coating equipment and the polymerization reactor, so it would be interesting to replicate the experiments in larger scale to see the real catalytic power of ZnGA films deposited by ALD.

6. References

1. L. Niinistö, M. Ritala and M. Leskelä, *Mater. Sci. Eng. B*, **41** (1996) 23.

2. M. Ritala and J. Niinistö. In *Chemical Vapour Deposition: Precursors, Processes and Applications*; A. C. Jones, and M. L. Hitchman, Eds.; The Royal Society of Chemistry: Cambridge, U.K. (2009) pp. 158–206.

3. V. Miikkulainen, M. Leskelä, M. Ritala, and R. L. Puurunen, *J. Appl. Phys.*, **113** (2013) 021301.

4. T. Hatanpää, M. Vehkamäki, I. Mutikainen, J. Kansikas, M. Ritala, and M. Leskelä, *Dalton Trans.*, **8** (2004) 1181.

5. D.-S. Kil, J.-M. Lee, and J.-S. Roh, *Chem. Vap. Deposition*, **8** (2002) 195.

6. M. Nieminen, T. Sajavaara, E. Rauhala, M. Putkonen, and L. Niinistö, J. Mater. Chem., **11** (2001) 2340.

7. K. Kukli, J. Ihanus, M. Ritala, and M. Leskelä, *Appl. Phys. Lett.*, **68** (1996) 3737.

8. T. Suntola and J. Antson, U.S. Patent 4058430 (1977).

9. M. T. Bohr, R. S. Chan, T. Ghani, and K. Mistry, *IEEE Spectrum*, **44** (2007) 29.

10. Y. Du and S. M. George, *J. Phys. Chem. C*, **111** (2007) 8509–8517.

11. S. M. George, B. Yoon, and A. A. Dameron, *Acc. Chem. Res.*, **42** (2009) 498–508.

12. T. Yoshimura, S. Tatsuura, and W. Sotoyama, *Appl. Phys. Lett.*, **59** (1991) 482–484.

13. M. Putkonen, J. Harjuoja, T. Sajavaara, and L. Niinistö, *J. Mater. Chem.*, **17** (2007) 664.

14. A. Kim, M. A. Filler, S. Kim, and S. F. Bent, *J. Am. Chem. Soc.*, **127** (2005) 6123–6132.

15. P. W. Loscutoff, H.-B.-R. Lee, and S. F. Bent, *Chem. Mater.*, **22** (2010) 5563–5569.

16. T. Yoshimura, S. Tatsuura, and W. Sotoyama, *Appl. Phys. Lett.*, **60** (1992) 268–270.

17. L. Nicole, C. Laberty-Robert, L. Rozes, and C. Sanchez, *Nanoscale*, **6** (2014) 6267.

18. D. Avnir , D. Levy, and R. Reisfeld , *J. Phys. Chem.*, **88** (1984) 5956–5959.

19. D. Avnir , V. R. Kaufman, and R. Reisfeld , *J. Non-Cryst. Solids*, **74** (1985) 395–406.

20. P. Judeinstein and C. Sanchez, *J. Mater. Chem.*, **6** (1996) 511–525.

21. A. Gorin, R. Copperwhite, S. Elmaghrum, C. McDonagh, and M. Oubaha, *Proc. of SPIE*, **8191** (2011) 81911Q-1.

22. K. Luo, S. Zhou, and L. Wu, *Thin Solid Films*, **517** (2009) 5974-5980.

23. M. Kusabe, H. Kozuka, S. Abe, and H. Suzuki, *J. Sol-Gel Sci. Technol.*, **44** (2007) 111.

24. H.-Y. Ma, T.-L. Wang, P.-Y. Chang, and C.-H. Yang, *Nanomaterials*, **6** (2016) 44.

25. C.-C. Chang, L.-P. Cheng, F.-H. Huang, C.-Y. Lin, C.-F. Hsieh, and W.-H. Wang, *J. Sol-Gel Sci. Technol.*, **55** (2010) 199–206.

26. Y. Lim, Y.-S. Park, Y. Kang, D. Y. Jang, J. H. Kim, J.-J. Kim, A. Sellinger, and D. Y. Yoon, *J. Am. Chem. Soc.*, **133** (2011) 1375–1382.

27. M. Fernandes, V. Zea Bermudez, R. Sá Ferreira, L. D. Carlos, A. Charas, J. Morgado, M. M. Silva, and M. J. Smith, *Chem. Mater.*, **19** (2007) 3892–3901.

28. D. Levy, *Chem. Mater.*, **9** (1997) 2666–2670.

29. A. N. Khramov, N. N. Voevodin, V. N. Balbyshev, and M. S. Donley, *Thin Solid Films.*, **447–448** (2004) 549–557.

30. L. Znaidi, *Mat. Sci. Eng. B*, **174** (2010) 18–30.

31. H. Kozuka. In *Handbook of sol-gel science and technology: Processing, characterization and applications*; S. Sakka, ed.; Kluwer Academic Publishers: New York, Boston, Dordrecht, London, Moscow (2007) pp. 275–311.

32. E. J. Kappert, D. Pavlenko, J. Malzbender, A. Nijmeijer, N. E. Benes, and P. A. Tsai, *SoftMatter*, **11** (2015) 882.

33. Y. Yoo and H. K. Jeong, *Chem. Commun.*, **21** (2008) 2441–2443.

34. Z.-Q. Li, L.-G. Qiu, T. Xu, Y. Wu, W. Wang, Z.-Y. Wu, and X. Jiang, *Mater. Lett.*, **63** (2009) 78–80.

35. S. Qiu, M. Xue, and G. Zhu, *Chem. Soc. Rev.*, **43** (2014) 6116–6140.

36. B. F. Hoskins and R. Robson, *J. Am. Chem. Soc.*, **111** (1989) 5962.

37. H. Li, M. Eddaoudi, M. O. Keeffe, and O. M. Yaghi, *Nature*, **402** (1999) 276–279.

38. M. Eddaoudi, J. Kim, N. Rosi, D. Vodak, J. Wachter, M. O'Keeffe, and O. M. Yaghi, *Science*, **295** (2002) 469–472.

39. N. Rosi, J. Eckert, M. Eddaoudi, D. Vodak , J. Kim, J. Wachter, M. O'Keeffe, and O. M. Yaghi, *Science*, **300** (2003) 1127–1129.

40. S. Hermes, F. Schröder, R. Chelmowski, C. Wöll, and R. A. Fischer, *J. Am. Chem. Soc.*, **127** (2005) 13744–13745.

41. Y. Liu, Z. Ng, E. A. Khan, H.-K. Jeong, C. Ching, and Z. Lai, *Microporous Mesoporous Mater*, **118** (2009) 296–301.

42. Z. Zhao, X. Ma, A. Kasik, Z. Li, and Y. S. Lin, *Ind. Eng. Chem. Res.*, **52** (2013) 1102–1108.

43. O. Guselnikova, P. Postnikova, R. Elashnikov, E. Miliutina, V. Svorcik, and O. Lyutakova, *Anal. Chim. Acta*, **1068** (2019) 70–79.

44. N. T. Tran, J. Kim, and M. R. Othman, *Microporous Mesoporous Mater.*, **285** (2019) 178–184.

45. S. R. Venna and M. A. Carreon, *J. Am. Cem. Soc.*, **132** (2010) 76–78.

46. J. Gascon, S. Aguado, and F. Kapteijn, *Microporous Mesoporous Mater.*, **113** (2008) 132–138.

47. S. Zhou, X. Zou, F. Sun, H. Ren, J. Liu, F. Zhang, N. Zhao, and G. Zhu, *Int. J. Hydrog. Energy*, **38** (2013) 5338–5347.

48. M. C. Petty. In *Langmuir-Blodgett Films*; G. Roberts, ed.; Springer US: New York, USA (1990) pp. 93–132.

49. J. A. Zasadzinski, R Viswanathan, L. Madsen, J. Garnaes, and D. K. Schwartz, *Science*, **263** (1994) 1726–1733.

50. S. Acharya, D. Bhattacharjee, J. Sarkara, and G. B. Talapatra, *Chem. Phys. Lett.*, **393** (2004) 1–6.

51. G. L. Gaines, Jr. In *Langmuir-Blodgett Films*; W. A. Barlow, ed.; Elsevier Scientific Publishing Company: Amsterdam, Oxford, New York (1990) pp. 1–7.

52. X.-L. Wang, Y.-L. Wang, W.-K. Miao, M.-B. Hu, J. Tang, W. Yu, Z.-Y. Hou, P. Zheng, and W. Wang, *Langmuir*, **29** (2013) 6537–6545.

53. M. Clement-León, E. Coronado, P. Delhaes, C. J. Góme-García, and C. Mingotaud, *Adv. Mater.*, **13** (2011) 547–577.

54. M. Jiang, T. Jiaoa, and M. Liu, *New J. Chem.*, **32** (2008) 959–965.

55. L. Liu, J. Yang, L.-X. Qiao, M. Chen, S.-Z. Liu, Z.-. Du, Z.-J. Zhou, and W.-Y. Wong, *J. Organomet. Chem.*, **694** (2009) 2786–2792.

56. G. K. Bhullar, R. Kaur, and K. K. Raina, *J. Appl. Polym. Sci.*, **132** (2015) 41386.

57. H. Usami, and S. Sasaki, *J. Photopolym. Sci. Technol.*, **26** (2013) 207–211.

58. D. M. Mattox. *Handbook of Physical Vapor Deposition (PVD) Processing*; William Andrew: Norwich, N.Y., USA (2010) pp. 1–36.

59. K. Bobzin, G. Hirt, N. Bagcivan, L. Khizhnyakova, and M. Evering, *J. Nanosci. Nanotechnol.*, **11** (2011) 8782–8785.

60. P. LeClair, G. P. Berera, and J. S. Moodera, *Thin Solid Films*, **376** (2000) 9–15.

61. D. E. Wolfe and J. Singh, *Surf. Coat. Technol.*, **124** (2000) 142–153.

62. N. Barreau , S. Marsillac, J. C. Bernède, T. Ben Nasrallah, and S. Belgacem, *Phys. Stat. Sol.*, **184** (2001) 179–186.

63. Y. Xiao, F.-X. Wang, J.-M. Yang, M.-R. Zhang, and G.-B. Pan, *Sci. Rep.*, **7** (2017) 9838.

64. S. Bonomi, D. Marongiu, N. Sestu, M. Saba, M. Patrini, G Bongiovanni, and Lorenzo Malavasi, *Sci. Rep.*, **8** (2018) 15388.

65. A. C. Jones and M. L. Hitchman. In *Chemical Vapour Deposition: Precursors, Processes and Applications*; A. C. Jones and M. L. Hitchman, Eds.; The Royal Society of Chemistry: Cambridge, U.K. (2009) pp. 1–36.

66. S.-J. Cho, I.-S. Bae, and J.-H. Boo, *Thin Solid Films*, **518** (2010) 6417–6421.

67. H. J. Seo, S.-H. Nam, S. Kim, and J.-H. Boo, *Appl. Surf. Sci.*, **354** (2015) 134–138.

68. Y.-S. Li, C.-H. Tsai, S.-H. Kao, I.-W. Wu, J.-Z. Chen, C.-I. Wu, C.-F. Lin, and I.-C. Cheng, *J. Phys. D: Appl. Phys.*, **46** (2013) 435502.

69. B. H. Lee, M. K. Ryu, S.-Y. Choi, K.-H. Lee, S. Im, and M. M. Sung, *J. Am. Chem. Soc.*, **129** (2007) 16034–16041.

70. A. A. Dameron, D. Seghete, B. B. Burton, S. D. Davidson, A. S. Cavanagh, J. A. Bertrand, and S. M. George, *Chem. Mater.*, **20** (2008) 3315–3326.

71. Q. Peng, B. Gong, R. M. VanGundy, and G. N. Parsons, *Chem. Mater.*, **21** (2009) 820–830.

72. B. H. Lee, V. R. Anderson, and S. M. George, *Chem. Vap. Deposition*, **19** (2013) 204–212.

73. B. H. Lee, V. R. Anderson, and S. M. George, *ACS Appl. Mater. Interfaces*, **19** (2014) 16880–16887.

74. O. Nilsen, K. B. Klepper, H. Ø. Nielsen, and H. Fjellvåg, *ECS Trans.*, **16**(4) (2008) 3–14.

75. K. B. Klepper, O. Nilsen, P.-A. Hansen, and H. Fjellvåg, *Dalton Trans.*, **40** (2011) 4636–4646.

76. K. Klepper, V. Miikkulainen, O. Nilsen, H. Fjellvåg, M. Liu, D. Dutta, and S. King, *MRS Proc.*, **1791** (2015) 15–20.

77. O. Nilsen, K. R. Haug, T. Finstad, and Helmer Fjellvåg, *Chem. Vap. Deposition*, **19** (2013) 174–179.

78. A. Hany, Z. D. Popovic, Chem. Mater., **16** (2004) 4522–4532.

79. A. Sood, P. Sundberg, and M. Karppinen, *Dalton Trans.*, **42** (2013) 3869–3875.

80. P. Sundberg and M. Karppinen, *Eur. J. Inorg. Chem.*, **6** (2014) 968–974.

81. B. Gong, Q. Peng, and G. N. Parsons, *J. Phys. Chem. B*, **115** (2011) 5930–5938.

82. E. Ahvenniemi and M. Karppinen, *Chem. Commun.*, **52** (2016) 1139–1142.

83. E. Ahvenniemi and M. Karppinen, *Chem. Mater.*, **28** (2016) 6260−6265.

84. M. Nisula and M. Karppinen, *Nano Lett.*, **16** (2016) 1276−1281.

85. L. Wang, C. Mou, Y. Sun, W. Liu, and Q. Deng, and J. Li, *Electrochim. Acta*, **173** (2015) 235−241.

86. J. F. M. Oudenhoven, L. Baggetto, and P. H. L. Notten, *Adv. Energy Mater.*, **1** (2011) 10−33.

87. E. Ahvenniemi and M. Karppinen, *Dalton Trans.*, **45** (2016) 10730–10735.

88. Z. Giedraityte, P. Sundberg, and M. Karppinen, *J. Mater. Chem. C*, **3** (2015) 12316–12321.

89. Z. Giedraityte, L.-S. Johansson, and M. Karppinen, *RSC Adv.*, **6** (2016) 103412–103417.

90. S. Eslava, L. Zhang, S. Esconjauregui, J. Yang, K. Vanstreels, M. R. Baklanov, and E. Saiz, *Chem. Mater.*, **25** (2013) 27–33.

91. K. Khaletskaya, S. Turner, M. Tu, S. Wannapaiboon, A. Schneemann, R. Meyer, A. Ludwig, G. Van Tendeloo, and R. A. Fischer, *Adv. Funct. Mater.*, **24** (2014) 4804–4811.

92. I. Stassen, M. Styles, G. Grenci, H. Van Gorp, W. Vanderlinden, S. De Feyter, P. Falcaro, D. De Vos, P. Vereecken, and Rob Ameloot, *Nat. Mater.*, **15** (2016) 304–310.

93. M. Krishtab, I. Stassen, T. Stassin, A. J. Cruz, O. O. Okudur, S. Armini, C. Wilson, S. De Gendt, and R. Ameloot, *Chem. Commun.*, **55** (2019) 10056–10059.

94. A. J. Cruz, I. Stassen, M. Krishtab, K. Marcoen, T. Stassin, S. Rodríguez-Hermida, J. Teyssandier, S. Pletincx, R. Verbeke, V. Rubio-Giménez, S. Tatay, C. Martí-Gastaldo, J. Meersschaut, P. M. Vereecken, S. De Feyter, T. Hauffman, and Rob Ameloot, *Chem. Mater.*, **31** (2019) 9462−9471.

95. K. B. Lausund and O. Nilsen, *Nat. Commun.*, **7** (2016) 13578.

96. K. B. Lausund, V. Petrovicab, and O. Nilsen, *Dalton Trans.*, **46** (2017) 16983–16992.

97. M. Ylilammi and T. Ranta-aho, Thin Solid Films, **232** (1993) 56–62.

98. O. M. E. Ylivaara and L. Kilpi, *J. Vac. Sci. Technol. A*, **35** (2017) 01B105.

99. K. Kukli, M. Kemell, H. Castán, S. Dueñas, H. Seemen, M. Rähn, J. Link, R. Stern, M. Ritala, and M. Leskelä, *ECS J. Solid State Sci. Technol.*, **7** (2018) P501–P508.

100. H. Seemen, M. Rähn, K. Kalam, T. Sajavaara, S. Dueñas, H. Castán, J. Link, R. Stern, K. Kukli, and A. Tamm, *ECS J. Solid State Sci. Technol.*, **7** (2018) **7** P402–P409.

101. D. C. Miller, R. R. Foster, Y. Zhang, S.-H. Jen, J. A. Bertrand, Z. Lu, D. Seghete, J. L. O'Patchen, R. Yang, Y.-C. Lee, S. M. George, and M. L. Dunn, *J. Appl. Phys.*, **105** (2009) 093527.

102. K. S. Han and M. M. Sung, *J. Nanosci. Nanotechnol.*, **14** (2014) 6137–6142.

103. K. Kukli, M. Ritala, and M. Leskelä, *J. Electrochem. Soc.*, **142** (1995) 1670–1675.

104. G. Maier, *Prog. Polym. Sci.*, **26** (2001) 3.

105. ZN4O FORMATION. V. Auger and J. Robin, *Compt. Rend.*, **178** (1924) 1546–1548.

106. S. J. Yang, J. Y. Choi, H. K. Chae, J. H. Cho, K. S. Nahm, and C. R. Park, *Chem. Mater.*, **21** (2009) 1893–1897.

107. L. T. L. Nguyen, C. V. Nguyen, G. H. Dang, K. K. A. Le, and N. T. S. Phan, *J. Mol. Catal. A-Chem.*, **349** (2011) 28–35.

108. S. Hermes, F. Schröder, S. Amirjalayer, R. Schmid, and R. A. Fischer, *J. Mater. Chem.*, **16** (2006) 2464–2472.

109. Y.-Q. Zheng, J.-L. Lin, and H.-L. Zhang, *Z. Kristallogr. NCS*, **215** (2000) 535–536.

110. J.-S. Kim, H. Kim, and M. Ree, *Chem. Mater.*, **16** (2004) 2981–2983.

111. M. Ree, J. Y. Bae, J. H. Jung, and T. J. Shin, *J. Polym. Sci.*, A **37** (1999) 1863.

112. M. Ree, Y. Hwang, J.-S. Kim, H. Kim, G. Kim, and H. Kim, *Catal. Today*, **115** (2006) 134.

113. L. Gao, Y. Luo, Y. Lin, T. Su1, R. Su, and J. Feng, *J. Polym. Res.*, **22** (2015) 220.